ALMA MATER STUDIORUM
UNIVERSITA’ DI BOLOGNA

SCUOLA DI INGEGNERIA E ARCHITETTURA
Sede di Forlì

Corso di Laurea in
INGEGNERIA AEROSPAZIALE
Classe LM-20

TESI DI LAUREA

in Spacecraft Attitude Dynamics and Control

Design and implementation of the ESEO spacecraft simulator

CANDIDATO
Alberto Lucci

RELATORE
Prof. Paolo Tortora

Anno Accademico 2014/2015
Sessione II

Contents

List of Figures

List of Tables

Sommario

Il lavoro di tesi si sviluppa nell'ambito del progetto ESEO (*European Student Earth Orbiter*), promosso dall'ESA (*European Space Agency*) al fine di formare ingegneri qualificati nell'ambito dei programmi spaziali europei.
Nei seguenti capitoli analizzeremo come simulare alcuni sottosistemi di ESEO. Primo fra tutti il Sottosistema Termico per valutare l'andamento delle temperature della strumentazione di bordo. A tal proposito risulterà necessario tenere in considerazione anche aspetti legati alla dinamica orbitale e di assetto al fine di calcolare i flussi dovuti all'ambiente spaziale.
Il passo successivo riguarderà la simulazione del Sottosistema di Potenza che modella l'abilità dello spacecraft di produrre e immagazzinare energia elettrica per il suo funzionamento.
Infine integreremo a tale simulatore un blocco Simulink che simula la capacità del satellite di comunicare con la Stazione di Terra attraverso segnali radio. Quest'ultimo step è stato progettato e validato durante il lavoro di preparazione alla tesi.

Abstract

The thesis work is developed under the *European Student Earth Orbiter* (ESEO) project supported by the *European Space Agency* (ESA) in order to help prepare a well-qualified space-engineering workforce for Europe's future.
In the following chapters we are going to analyse how to simulate some ESEO subsystem. First of all, the Thermal Subsystem that evaluates the temperature evolution of on-board instruments. For this purpose, simulating also the orbital and attitude dynamics of the spacecraft, it is necessary in order to evaluate external environmental fluxes.
The Power Subsystem will be the following step and it models the ability of a spacecraft to produce and store electrical energy.
Finally, we will integrate in our software a block capable of simulating the communication link between the satellite and the Ground Station (GS). This last step is designed and validated during the thesis preparation.

Introduction

The thesis involves the design of a first simulator of the ESEO satellite that is also able to communicate with the GS through radio signals.
The starting point was a Power simulator of ESEO already implemented in Simulink. It contained aspects related to the modelling of the thermal subsystem (only external panels), the orbital and attitude dynamics.
The contribution given by the present work can be summarized as follows:

- Development of a detailed thermal model based on the informations provided by *SITAEL SpA*, Prime Contractor of the ESEO project. It is modelled, using the MATLAB based Simscape programming language, as a thermal network of nodes that communicate through radiative and conductive links;

- Modification of the power simulator, mainly as concerns the modelling of the solar panels;

- Integration of the different sub-blocks (interface, thermal, power and orbital) into one single simulator. In particular the first, implemented and validated during the thesis preparation, simulates a system capable of receiving a message from the GS, converting it in a specific request and sending the correct response, interacting with the spacecraft simulator.

In the end, the thesis is organized in order to analyse and verify the accuracy of the blocks mentioned above. After a brief introduction of the ESEO mission, the applied theory and the space environmental, in chapter *ESEO Thermal model* and *ESEO Power Simulator* the logic behind the design of the thermal and power simulator is reported, respectively. *Interface Block* is a summary of the thesis preparation work for a better comprehension of how the spacecraft communicates with the GS and how this behaviour is modelled in the simulator.

ESEO mission

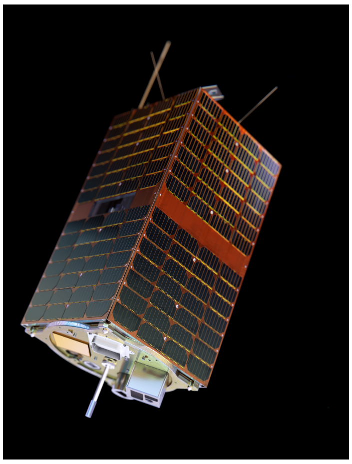

Figure 1: ESEO model [1]

The European Student Earth Orbiter is a micro-satellite mission to *Low Earth Orbiter* (LEO). It is being developed, integrated and tested by European university students, as an ESA Education Office project, in order to help prepare a well-qualified space-engineering workforce for Europe's future.

3.1 Mission objectives

ESEO satellite has the following mission objectives [7]:

- to take pictures of the Earth and/or other celestial bodies from Earth orbit for educational outreach purposes through the use of a micro camera (uCAM) operating in the visible spectrum;

- to provide dosimetry and space plasma measurement in Earth orbit and its effect on satellite components through two instruments: plasma diagnostic probe (LMP) and tri-dimensional dosimeter instrument (TRITEL);

- to test technologies for future educational satellite missions such as a GPS receiver for orbit determination and a De-Orbit Mechanisms (DOM). Satellite will also carry on board a dedicated S-band transmitter (HSTX), in order to provide high speed datalink for payload data transmission, and a payload proposed by AMSAT community for radio-amateur community.

3.1.1 ESEO target orbit

The target orbit for ESEO mission ia a circular *Sun-Synchronous Orbit* (SSO) 10:30 LTAN [7] and the orbital parameters are reported in Table 1.

3.2 Spacecraft architecture

The ESEO platform architecture is based on both ALMASat-EO and ALMASat-1 heritage. Two modules, namely the *Bus Module* (BM) and the *Payload Module* (PM), contains all the subsystems

Orbital Parameters	**Mean System of Date**
Semi-major axis	6904.82699 km
Eccentricity	0.00134790°
Inclination	97.47884°
Ascending Node	137.34203°
Argument of Perigee	67.74183°
True Anomaly	292.25995°

Table 1: ESEO orbital parameters

and payloads. According to Figure 2 [1] and 3, in the BM most of the subsystems and their units are arranged inside aluminum trays in order to provide a physical separation, flexibility and reduced MAIN efforts; while in the PM, most of the payloads, are arranged in sectors.

3.2.1 Bus module

The tray arrangement of ALMASat-EO has been directly applied without modifications and so, the current platform, is composed by [8]:

- **Tray 1**
  It contains the cold-gas MicroPropulsion System (MPS) of the AOCS capable to provide orbit control maneuvers with 3 m/s of ΔV. Thrusters are aligned with the orbital velocity and both orbiting and de-orbiting maneuvers can be performed;

[1] The origin of the reference frame is located at the geometrical center of the bottom plate. X axis is aligned with the tangential orbital velocity while Z in the zenith pointing.

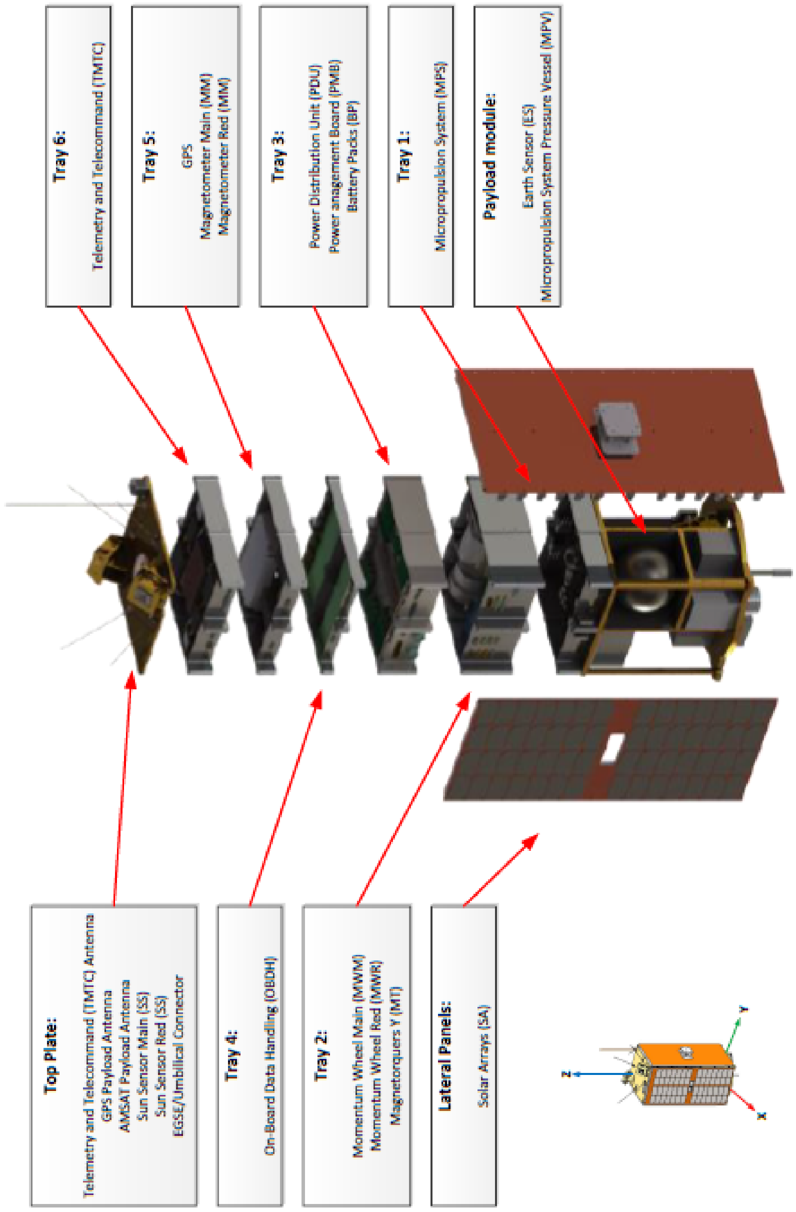

Figure 2: ESEO platform layout [2]

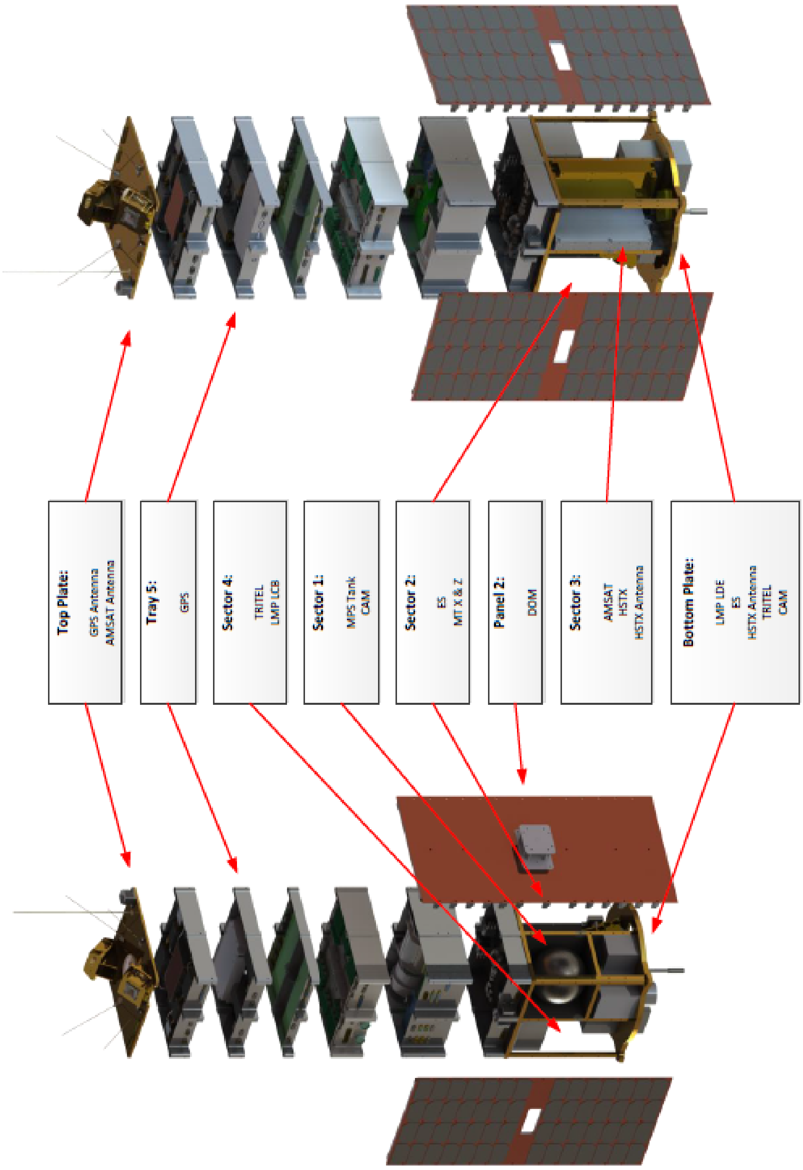

Figure 3: ESEO payloads layout [8]

- **Tray 2**
  It contains the redundant Momentum Wheels (MWM and MWR) and has a double overall height in order to contain the overall MWs envelope and a couple of redundant MagneTorquers (MT) acting on the Y-axis;

- **Tray 3**
  It contains the main components of the Power System (PS) namely the Power Management Board (PMB), the Power Distribution Unit (PDU) and the battery packs (BPs). Each unit is installed inside a dedicated aluminum frame, namely: BP inside Tray 3-1, PMB inside Tray 3-2 and PDU inside Tray 3-3;

- **Tray 4**
  It contains the *On-Board Data Handling* (OBDH) that is the central node for both logical and physical data connections of the platform subsystem;

- **Tray 5**
  It contains the couple of magnetometers and relevant electronics as well as the GPS receiver (considered as a payload in the context of the ESEO program);

- **Tray 6**
  It contains the overall TeleMetry and TeleCommand subsystem (TMTC);

- **Lateral panels**
  They provide support for the Solar Arrays (SA) and, considering the specific SSO orbit, the panel located on the +Y direction is not covered by solar cells and it is used as a radiator in order to better dissipate heat inside the spacecraft. Finally, DOM is installed on the same panel in order

to reduce as much as possible its effect on the nominal power production caused by solar cells shadowing;

- **Top plate**
  The Sun Sensors (SS), UHF antenna array, GPS and AMSAT payloads antenna systems are installed on the top plate. Moreover, since it provides easy accessibility during ground operations, the EGSE/umbilical connector of the spacecraft is located on this plate;

3.2.2 Payload module

The concept of composite payload module was introduced and combined with the classical tray-based bus module in order to provide room for payloads, improve accessibility during ground operations and, in general, improve system flexibility and adaptability to a wide range of payloads [14].
Except for GPS, this module contains all the payloads that will be useful to fulfil the mission objectives. In particular all the payloads requiring external accessibility to the nadir pointing face of the spacecraft are located in the bottom plate. They include: LMP, uCAM, TRITEL and HSTX. Also the Earth Sensor (ES) is installed on the bottom place requiring visibility to the earth.

Spacecraft heat transfer

Heat transfer can be describe as the *thermal energy in transit due to a spatial temperature difference* [3].
Conduction, radiation and convection are the heat transfer mode and, a combination of them, can be used to describe the flow of thermal energy into, out of and within a spacecraft.

4.1 Conduction

Conduction is the transfer of energy through a material as result of interaction between particles in that material. The time rate of heat transfer, due to this mode, is described by the *Fourier's Law* and, in particular the differential form of it, expressed as:

$$\vec{q} = -k\nabla T \tag{4.1}$$

where the local heat flux density $\vec{q}[\frac{W}{m^2}]$ is equal to the product of the material's thermal conductivity $k[\frac{W}{mK}]$ and the negative local temperature gradient $\nabla T[\frac{K}{m}]$. The minus sign is a consequence of the fact that heat is transferred in the direction of decreasing temperature.

4.2 Convection

In space, due to the extremely low residual pressure, the heat transfer with the external environmental happens only through the radiation mode; convection can be neglected.
However, for the sake of completeness, we recall here that it represents the transfer of heat between a solid and a neighbour fluid. In particular we have *natural convection* when the fluid motion is due to its internal density gradient; *forced convection* when the fluid motion is forced by an external force.

4.3 Radiation

Heat transfer by conduction and convection requires the presence of a temperature gradient in some form of matter. In contrast, heat transfer by thermal radiation requires no matter [3].
This mode involves the emission of electromagnetic waves from all matter that has a temperature grater than absolute zero and, in particular, in case of a *blackbody* the total emissive power is governed by the *Stefan-Boltzmann's Law*:

$$E_b = \sigma T^4 \tag{4.2}$$

where $E_b[\frac{W}{m^2}]$ is the amount of energy per unit of time per unit of area, integrated over all wavelengths, $\sigma[\frac{W}{m^2 K^4}]$ is the Stefan-Boltzmann constant and $T[K]$ is the temperature.
A blackbody is *a body which absorbs all energy that reaches it and reflects nothing* [4]; of course, a real surface is not a perfect absorbers or emitters such that, the emissive power is scaled by a proportionality term ϵ:

$$E_b = \epsilon\sigma T^4 \tag{4.3}$$

The *emissivity* ($0 \leq \epsilon \geq 1$) represents *how efficiently a surface emits energy relative to a blackbody* [3] and depends strongly on the

surface material and finish. Moreover emissivity is also a function of wavelength and direction but under the hypothesis of *diffuse* ($\frac{\delta\epsilon}{\delta\lambda} = 0$) and *grey* surface it can be considered a constant.
Other important properties of a real surface are the absorptivity (α: fraction of the incident light on a surface that is absorbed), reflectivity (ρ: fraction of the incident light on a surface that is reflected) and transmissivity (τ: fraction of the incident light on a surface that is transmitted). Since energy can be neither created nor be destroyed we have the following equality:

$$\alpha + \rho + \tau = 1 \tag{4.4}$$

Moreover if the surface is *opaque* ($\tau = 0$) and if it is in thermal equilibrium, *Kirchoff's Law* implies that:

$$\alpha = \epsilon \tag{4.5}$$

In order to complete this brief resume of the thermal radiation we have to introduce the concept of *View Factor* (F_{ij}) also called *Configuration* or *Shape Factor*. It is the *fraction of the radiation leaving surface i that is intercepted by surface j* [3]. This pure geometrical factor is fundamental in order to evaluate the net rate of radiative energy between two different surfaces; it can be calculated according to Equation 4.6 and the meaning of the variables in it are reported in Figure 4.

$$F_{ij} = \frac{1}{A_i} \int_{A_i} \int_{A_j} \frac{\cos\theta_i \cos\theta_j}{\pi S^2} dA_i dA_j \tag{4.6}$$

An important result in regard to the view factor is that all the energy leaving a generic surface i reaches the surfaces in the neighborhood of it (Equation 4.7).

$$\sum_{k=1}^{n} F_{ik} = 1 \tag{4.7}$$

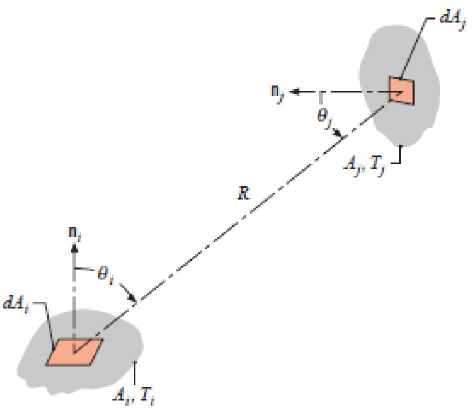

Figure 4: Geometry for calculating the view factor between two differential areas [3]

In closing the *reciprocity relation* (Equation 4.8) is very useful in determining one view factor from knowledge of the other:

$$A_i F_{ij} = A_j F_j \tag{4.8}$$

while, in case of composite surface, the *superposition rule* becomes an important instrument:

$$F_{i(jk)} = F_{ij} + F_{ik} \tag{4.9}$$

the view factor from a surface i to a surface $(j+k)$ is equal to the sum of the view factors from surface i to the parts j and k.
For practical purposes Equation 4.6 is not used to evaluate view factors because, also a complex case, can be brought back, together with Equation 4.7, 4.8 and 4.9, to a mix of configurations available in a specific catalogue [13].
An example of this is as follow: in Figure 5 is reported a box with

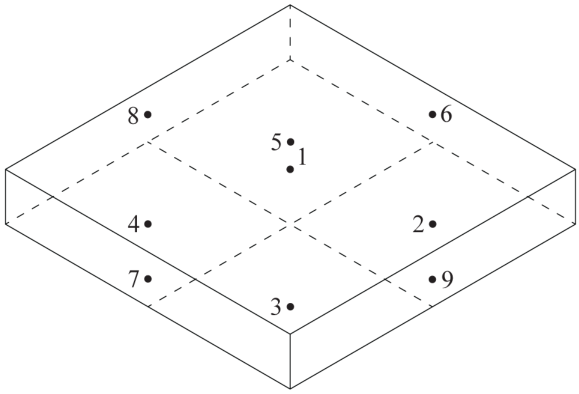

Figure 5: Example for determining view factors among surfaces

the bottom panel divided in four equal parts. For a better comprehension, each sides is identified with a number. According to this case only two useful relations are necessary: the first (Section C-14 of [13]) models the view factor between *two finite rectangles of same length, having one common edge, and at an angle of* 90° *to each other* while the second (Section C-11 of [13]) between *identical, parallel, directly opposed rectangles.* However, applying the conservation of energy and the reciprocity rule, only one of these equations is useful for evaluating view factors that do not involve the surfaces of the bottom panel. For these, additional observations are necessary, in fact, if we consider the bottom panel as a unique surface:

$$F_{1(2345)} = 1 - F_{11} - F_{16} - F_{17} - F_{18} - F_{19}$$

where, apart from F_{11} that is zero under the hypothesis of *flat surface*, the other view factors are known according to the previous analysis.
From the superposition rule:

$$F_{1(2345)} = F_{12} + F_{13} + F_{14} + F_{15}$$

and the symmetry of the scheme:

$$F_{12} = F_{13} = F_{14} = F_{15}$$

we have that:

$$F_{12} = F_{13} = F_{14} = F_{15} = \frac{F_{1(2345)}}{4}$$

The view factors between the surface identified by number 8 and one of the division of the bottom plate can be evaluated with some simple geometrical consideration that are valid also for the other lateral sides. Using the relation in Section C-14 of [13] it is possible to evaluate $F_{8(45)}$ and $F_{8(2345)}$. For the symmetry:

$$\begin{aligned} F_{84} &= F_{85} \\ F_{82} &= F_{83} \end{aligned}$$

and from the superposition rule:

$$\begin{aligned} F_{8(45)} &= F_{84} + F_{85} \\ F_{8(2345)} &= F_{82} + F_{83} + F_{8(45)} \end{aligned}$$

we have that:

$$\begin{aligned} F_{84} = F_{85} &= \frac{F_{8(45)}}{2} \\ F_{82} = F_{83} &= \frac{F_{8(2345)} - F_{8(45)}}{2} \end{aligned}$$

Space environment

A spacecraft in LEO receives radiant thermal energy from three sources and reflects it to deep space. The three primary sources are the incoming solar radiation, Earth albedo radiation and Earth infrared radiation (Figure 6).

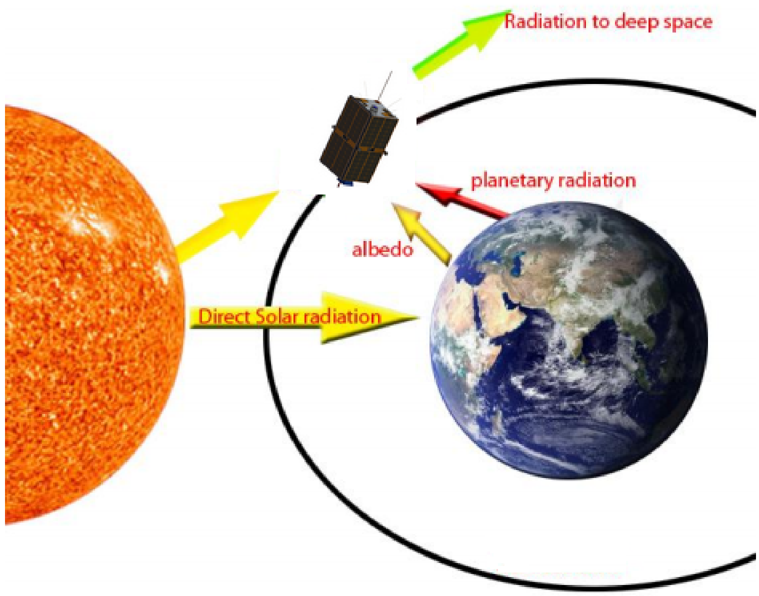

Figure 6: Thermal environment for a spacecraft in LEO

Moreover, the internal dissipated power in electronic components due to Joule effect must be considered as another thermal source.

5.1 Incoming solar radiation

Sun is considered as a blackbody and so, its total emissive power, can be modelled according to Equation 4.2; this value is influenced by two factors. First, *the amount of radiant energy emitted by the Sun is known to vary slightly throughout the 11-year solar cycle.* Second, *the slightly elliptical orbit of the Earth about the Sun results in a variation in the solar flux incident on the Earth or upon an Earth orbiting spacecraft* [5]. According to this we have a mean value, also called as *solar constant* (Φ_s) equal to $1367\frac{W}{m^2}$ that represents *the radiation that falls on a unit area of surface normal to the line from the Sun, per unit time and outside from the atmosphere, at one astronomical unit* [5].
Since the Sun distance is extremely large we can suppose that the rays coming from it are parallel and so, a generic face of the spacecraft absorbs a quote of the incident solar flux (Q_{Sun}) equal to:

$$Q_{Sun} = \alpha A \Phi_s \cos\theta \tag{5.1}$$

where θ is the angle between the vector normal to the face and the solar flux vector.

5.2 Earth albedo radiation

Albedo is *the fraction of incident solar energy reflected (or scattered) by a planet back into space* [5] and its flux is relatively more complex to evaluate because it depends on many parameters such as satellite's position on the orbit, Earth view factor and so on.

The contribution of the albedo radiation is:

$$Q_{Albedo} = \alpha F_{al} F_{12} Al \Phi_s \tag{5.2}$$

where F_{al} is the *albedo visibility factor*, F_{12} is the view factor between satellite and Earth and Al is the *albedo coefficient*.
About F_{12}, compared to the large size of the Earth, a surface of a spacecraft can be approximated as an infinitesimal area dA_1 who's normal vector makes a generic angle θ, with respect to a straight line between dA_1 and the center of a sphere of radius r. If h is the distance from the Earth to the spacecraft and r is the Earth medium radius (Figure 7), defining $H = \frac{h}{r}$ and $\Phi = \arcsin(\frac{1}{H})$, the view factor between satellite and Earth can be modelled with the following equations:

- When the spacecraft surface can see the entire Earth-disk $(\theta \leq \frac{\pi}{2} - \Phi)$
$$F_{12} = \frac{\cos\theta}{H}$$
- When the spacecraft surface can partially see the Earth-disk $(\frac{\pi}{2} - \Phi < \theta \geq \frac{\pi}{2} + \Phi)$
$$F_{12} = \frac{1}{2} - \frac{1}{\pi} \arcsin[\frac{(H^2-1)^{\frac{1}{2}}}{H\sin\theta}] + \frac{1}{\pi H^2} \cos\theta \arccos[-((H^2-1)^{\frac{1}{2}}) \cot\theta] - (H^2-1)^{\frac{1}{2}} [1 - H^2 \cos^2\theta]^{\frac{1}{2}}$$
- When the spacecraft do not see the Earth $(\theta > \frac{\pi}{2} + \Phi)$
$$F_{12} = 0$$

5.3 Earth infrared radiation

For the simple fact that Earth has a temperature different from the absolute zero, it emits thermal radiation in infrared wavelength

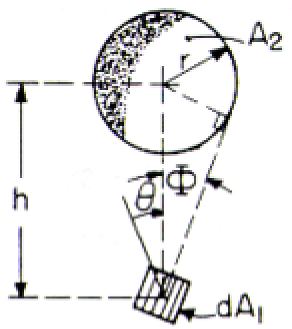

Figure 7: Arbitrarily oriented differential planar element to a sphere [13]

bands. This source is not constant over the globe but it has highest values in tropical and desert regions (these lands receive the maximum solar heating) and decrease with latitude.
For the purpose of spacecraft thermal analysis, Earth irradiates as a blackbody at temperature T_E and the heat exchange with the Earth surface is [6]:

$$Q_{Earth} = \sigma\epsilon F_{12}(T_E^4 - T^4) \tag{5.3}$$

where ϵ and T are the emissivity and the temperature of a generic surface, respectively.

5.4 Deep space

A generic surface of the spacecraft exchanges heat with the deep space, modelled as an ideal source at constant temperature of $4K$ (T_{space}), according to this equation [6]:

$$Q_{Space} = \sigma\epsilon(1 - F_{12})(T^4 - T_{space}^4) \tag{5.4}$$

5.5 For a surface with solar cells?

For the sake of completeness, Equation 5.1 and 5.2 are referred to a generic surface while, from the ESEO satellite point of view, it is convenient to consider how they change for a solar panel. Since part of the direct solar radiation is converted into electrical power the contribution of the incoming solar radiation and of the Earth albedo radiation have to be modified as follows [6]:

$$Q_{Sun} = \alpha(1-\eta_{eq})A\Phi_s\cos\theta$$
$$Q_{Albedo} = \alpha(1-\eta_{eq})F_{al}F_{12}Al\Phi_s$$

where η_{eq} is an equivalent efficiency because it takes into account the effective portion of solar panel area covered by solar cells. Since an ESEO solar panel is made by $GaAs$ (α_G, η_G and A_G) and $Kapton$ (α_K, $\eta_K(=0)$ and A_K), it is possible to derive an equation for the equivalent efficiency, considering the power balance of the incoming solar radiation:

$$\alpha(1-\eta_{eq})cos\theta J(A_K+A_G) = \alpha_K(1-\eta_K)cos\theta JA_K + \alpha_G(1-\eta_G)cos\theta JA_G \tag{5.5}$$

where η_G is the (temperature dependent) efficiency of the solar cell and it has been inserted in the Simulink model by importing a lookup table (Table 2), computed on the basis of a specific datasheet.

Temperature [K]	**Solar Efficiency** (η_G)
223	0.319
243	0.310
263	0.299
273	0.294
283	0.289
301	0.279
303	0.278
323	0.267
343	0.255
363	0.244
383	0.232
403	0.219
423	0.206

Table 2: Temperature vs Solar efficiency (lookup table) [15]

ESEO Thermal model

This represent the core of the thesis work and all the steps followed to develop the model are reported in the following sections.

6.1 How to model it

Its mission is to provide accurate predictions of the evolution with time of the temperatures in selected points of the satellite.
Two widespread approaches to the thermal simulation of spacecraft exist [9]:

- **Interpolation method**
  It operates by carrying some kind of interpolation over a finite set of selected, typical scenarios for which the thermal behaviour is known. The model is very simple and its implementation straightforward but there is an interpolation error for those unknown contexts and extrapolation will produce uncertain prediction;

- **Integration method**
  First the thermal subsystem is discretised in a network of *nodes* and *links* (*nodalisation* phase); second, the heat transfer equations are applied to this network, thus yielding a system of differential equations that can be solved using a numerical integrator. The development of a thermal model

is a complex task that requires expertise and time but the advantages are the high precision attainable and the validity for non-nominal situations (e.g failures)
This approach is employed in the thermal analysis tool of ESA (ESATAN-*European Space Agency Thermal ANalyser*).

According to this we decide to choose the second approach and to simulate the thermal subsystem with *Simscape*. It *provides an environment for simulating physical systems spanning mechanical, electrical, hydraulic, and other physical domains* [10]. In particular, for our purpose, Simscape contains thermal building blocks for modelling conductive and radiative heat transfer as well as the thermal mass of elements and measuring the amount of temperature change.

6.1.1 Nodalisation phase

As previously anticipated, this phase consists in discretising of the system in a network. It is also called *Lumped Parameter Network* (LPN) because *the continuous parameters of the thermal system have been "lumped" into the discrete set of the nodes and links* [9].

Node types

A node (an isothermal volumes where heat can be stored) is characterized by its thermal capacitance and, optionally, by a heat source. It can be of these types [11]:

- **Diffusion node**: it has a finite capacitance and is used to represent normal material nodalization. In Simscape, this type of node is implemented by the *thermal mass* block (Figure 8);

- **Arithmetic node**: it has zero capacitance and is a physically unreal quantities. An arithmetic node can represent

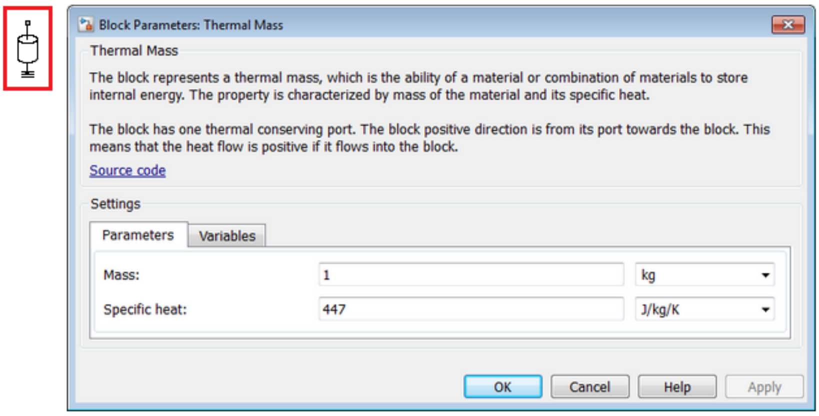

Figure 8: Thermal mass in Simscape

elements which have small capacitance values in comparison to the large majority of the other nodes;

- **Boundary node**: it has an infinite capacitance and is used to represent constant temperature sources (e.g. deep space) within a thermal network.

However, in Simscape an heat source is implemented by the *ideal heat flow source* block (Figure 9).

Link types

A link is a path between two nodes that allows heat to flow from one to the other [9] and can be:

- **Conductive link**
  In Simscape, it is implemented by the *conductive heat transfer* block (Figure 10). A conductive link is characterized by its thermal conductance; the flow between two generic nodes

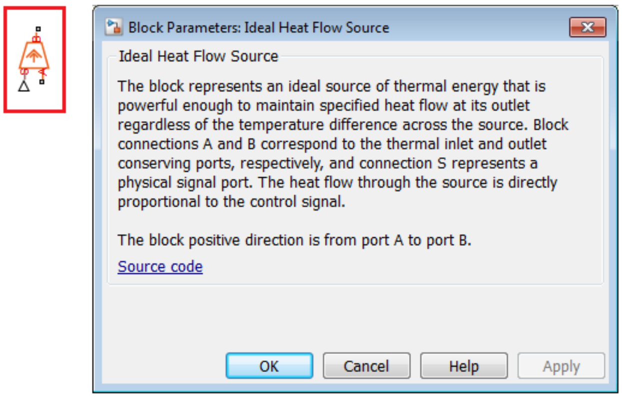

Figure 9: Ideal heat flow source in Simscape

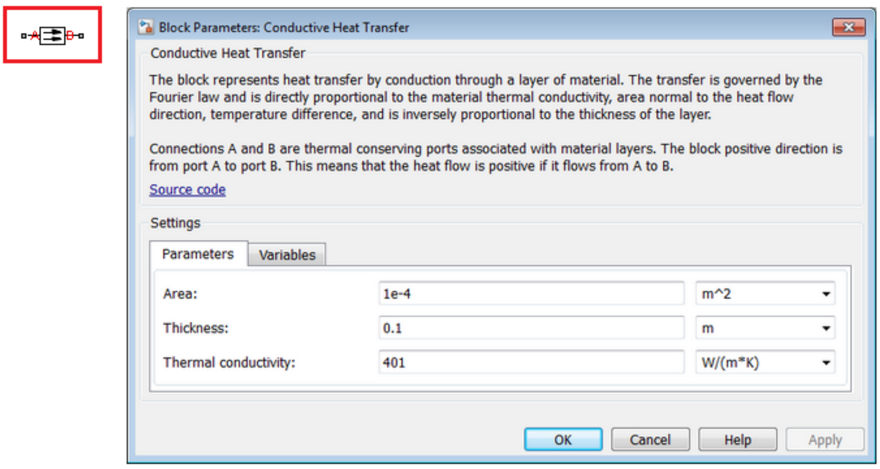

Figure 10: Conductive heat transfer in Simscape

i and j can be modelled in the following way:

$$Q_{Cond} = G_{ij}(T_j - T_i) \tag{6.1}$$

where $G_{ij}[\frac{W}{K}]$ is the conductance of the conductive link between nodes i and j. This relation derives from the differential equation (4.1) when integrated for a homogeneous material of 1-D geometry between two endpoints at a constant temperatures.
The use of the word "conductance" is not accidental; in fact *thermal and electrical systems are two such analogous systems* [11] and this allows the engineer to utilize the widely known basic laws for balancing electrical network. According to this two or more parallel conduction paths between nodes (Figure 11) may be summed to create an equivalent conductance G_T. Otherwise two or more series conduction

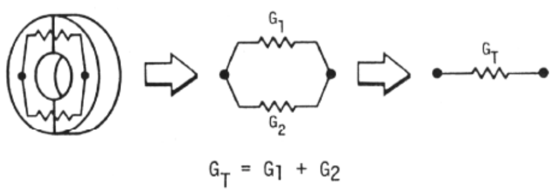

Figure 11: Parallel conductor flow paths [11]

paths between nodes may be combined to create one conductor value:

$$G_T = \frac{1}{\frac{1}{G_1} + \frac{1}{G_2} + \dots} \tag{6.2}$$

This may be helpful in computing the equivalent conductance between two dissimilar shaped or dissimilar nodes (Figure 12).
Conduction not only transfers heat within an object, but also

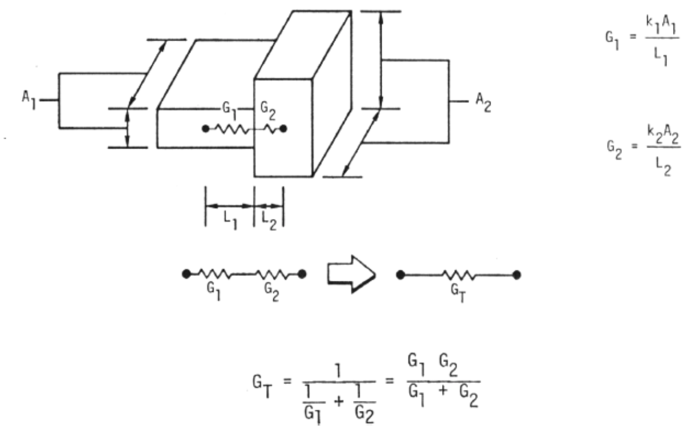

Figure 12: Series conductor flow paths [11]

between objects that have touching surfaces. In this case, conduction is characterized by a term called *contact conductance* (G_{cont}) which basically accounts for the reduced efficiency in the heat transfer due to imperfect surface contact. So, it is necessary to clarify that the relations in Figure 11 and 12 are valid under the hypothesis of perfect contact, i.e. $G_{cont} = 0$.

- **Radiative link**
  In Simscape, a radiative link is implemented by the *radiative heat transfer* block (Figure 13). A radiative link is characterized by its *radiative exchange factor* and, respect the conductive case, the flow between two nodes is proportional to the fourth power of the temperature:

$$Q_{Rad} = \sigma R_{ij}(T_j^4 - T_i^4) \tag{6.3}$$

where $R_{ij}[\frac{W}{K^4}]$ is the radiative exchange factor between nodes

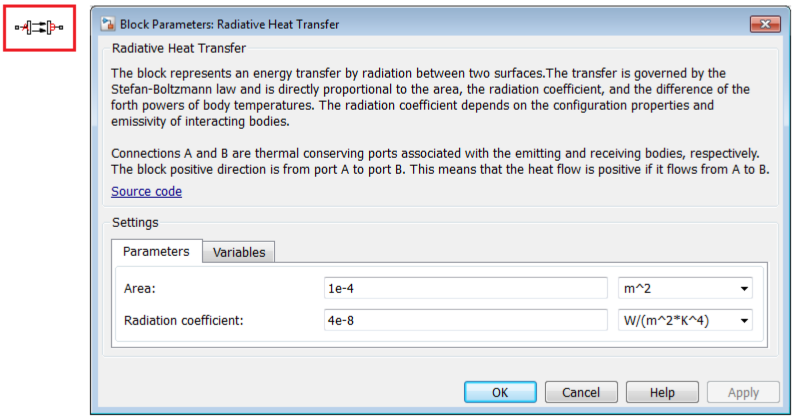

Figure 13: Radiative heat transfer in Simscape

i and j.
The computation of R_{ij} is quite complicated because it provides not only geometrical information but also thermal-optical properties of the nodes. In order to model this parameter it is possible to follow two different methods: *Gebhart method* (Section 6.1.3) and *Net-radiation method*. We decide to choose the first because it is considered to be the method with the least chance of error and the most direct way to calculate R_{ij} between surfaces.

6.1.2 Integration phase

Applying Equation 6.1 and 6.3 to the thermal network we obtain a non-linear system of differential equations, one for each node, of the form [9]:

$$C_i \frac{dT_i}{dt} = \sum_{i \neq j} G_{ij}(T_j - T_i) + \sum_{i \neq j} \sigma R_{ij}(T_j^4 - T_i^4) + Q_i, \quad i, j = 1, \ldots, N \qquad (6.4)$$

where N is the number of nodes in the network, $C_i[\frac{J}{K}]$ and $Q_i[W]$ the capacitance and the heat source of node i respectively. Integrating this system is possible to evaluate, at different times, the temperatures of each node of the LPN.
The integration phase is very important in order to obtain the target of a thermal subsystem but, from Simscape point of view, it is automatically fulfilled once we define the thermal network.

6.1.3 Gebhart method

The Gebhart method describes the radiative heat transfer in terms of heat coming from one surface and absorbed by another, including all reflections and it is valid under the grey body assumption and in case of an *enclosure* (an envelope of solid surfaces or open areas that completely surrounds a generic surface).
In order to consider all reflections we have to pass from the concept of view factor to the *grey body factor* (B). The first, already analysed in Section 4.3, quantifies the fraction of energy emitted from one surface that arrives at another surface *directly* while the second considers *all possible paths*. The Gebhart factor is defined as:

$$B_{ij} = \frac{Energy\ absorbed\ at\ A_j\ originating\ as\ emission\ at\ A_i}{Total\ radiation\ emitted\ at\ A_i}$$

From a mathematically point of view, for diffuse radiation and reflection, the Gebhart factors are given by [12]:

$$\sum_{k=1}^{N}(F_{ik}\rho_k - \delta_{ij})B_{kj} + F_{ij}\epsilon_j = 0, \quad i,j = 1,\dots,N \tag{6.5}$$

where i is the node of departing energy, j is the node of destination energy and δ_{ij} is the Kronecker's delta.
From the Equation 4.4, considering Kirchhoff's law (Equation 4.5)

and opaque surfaces, Equation 6.5 is reduced to:

$$\sum_{k=1}^{N}(F_{ik}(1-\epsilon_k)-\delta_{ij})B_{kj}+F_{ij}\epsilon_j=0, \quad i,j=1,\ldots,N \qquad (6.6)$$

This relation can be expressed as a matrix equation to isolate the Gebhart factors:

$$\begin{bmatrix} F_{11}(1-\epsilon_1)-1 & F_{12}(1-\epsilon_2) & \ldots & F_{1N}(1-\epsilon_N) \\ F_{21}(1-\epsilon_1) & F_{22}(1-\epsilon_2)-1 & \ldots & F_{2N}(1-\epsilon_N) \\ \vdots & \vdots & & \vdots \\ F_{N1}(1-\epsilon_1) & F_{N2}(1-\epsilon_2) & \ldots & F_{NN}(1-\epsilon_N)-1 \end{bmatrix} \begin{bmatrix} B_{11} & \ldots & B_{1N} \\ B_{21} & \ldots & B_{2N} \\ \vdots & & \vdots \\ B_{N1} & \ldots & B_{NN} \end{bmatrix} = - \begin{bmatrix} F_{11}\epsilon_1 & \ldots & F_{1N}\epsilon_N \\ F_{21}\epsilon_1 & \ldots & F_{2N}\epsilon_N \\ \vdots & & \vdots \\ F_{N1}\epsilon_1 & \ldots & F_{NN}\epsilon_N \end{bmatrix}$$

Writing in a compact form, we can solve for the Gebhart factors by:

$$\begin{aligned} [F_\rho]\,[B] &= -\,[F_\epsilon] \\ [B] &= [F_\rho]^{-1}\,[F_\epsilon] \end{aligned} \qquad (6.7)$$

The final step of the method analysed in this section is to turn the Gebhart factor into the radiative exchange factor:

$$R_{ij}=\epsilon_i A_i B_{ij}=\epsilon_j A_j B_{ji} \qquad (6.8)$$

In this equation we can see that, also for the B_{ij}, it is possible to define a sort of reciprocity relation. Another relationship is found by nothing that all the energy emitted by a surface i must be ultimately absorbed within the enclosure, thus:

$$\sum_{k=1}^{N} B_{ik}=1 \qquad (6.9)$$

6.2 Applying these concepts for the ESEO satellite

An accurate thermal subsystem is the natural consequence of a correct thermal network, essentially composed of nodes and links between these.

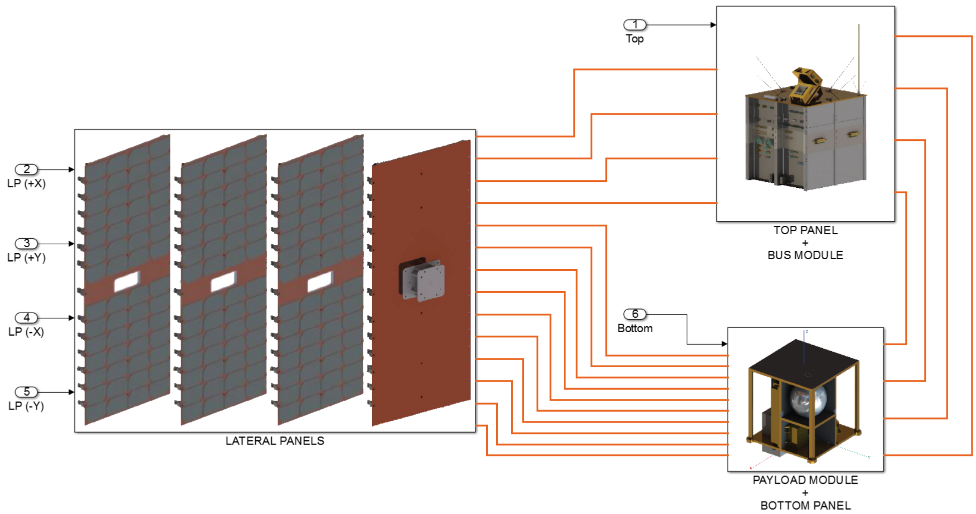

Figure 14: ESEO thermal model

6.2.1 Definition of nodes

First of all it is important to underline that the reason for the choice of the nodes will be clearer when we will analyse the section related to the radiative links (Section 6.2.2).

The LPN, implemented in the ESEO thermal model, is characterized by about 90 diffusion nodes whose mass and specific heat have been assigned according to data from the ESEO mission documentation, [14] and [15], respectively.

Bus module

In Section 3.2 we discovered that BM is composed by a series of stacked aluminum trays (Figure 15).
Two types of tray configurations have been implemented:

- **Configuration A**
  This configuration is characterized by an aluminum bottom plate integrated into the tray structure and it is applied for Tray 3,4 and 6;

- **Configuration B**
  It is used for all other trays and it consists of a removable composite bottom plate.

Quite apart from the different configurations, a tray is modelled with five nodes: one for each lateral side (Side (*Location*)) and one for the bottom plate (Figure 16).
The difference in case of trays with configuration B is only related to the nomenclature of the nodes (Figure 17). We have: Side_n (*Location*) for the lateral sides, where n is the number of the specific subdivision; *Bottom* or *Middle* for the bottom plate of the tray or of the internal frame respectively. The bottom plate of Tray 1 (and also the Bottom panel) is divided in four parts, each of them modelled with a node (Figure 18). Instead the Top panel is considered like a single node.
Moreover, in order to have a valid but, at the same time, not so complex thermal model, we decide that every subsystems, payloads or units, included in a generic tray, are modelled with the same node of the relative bottom plate.

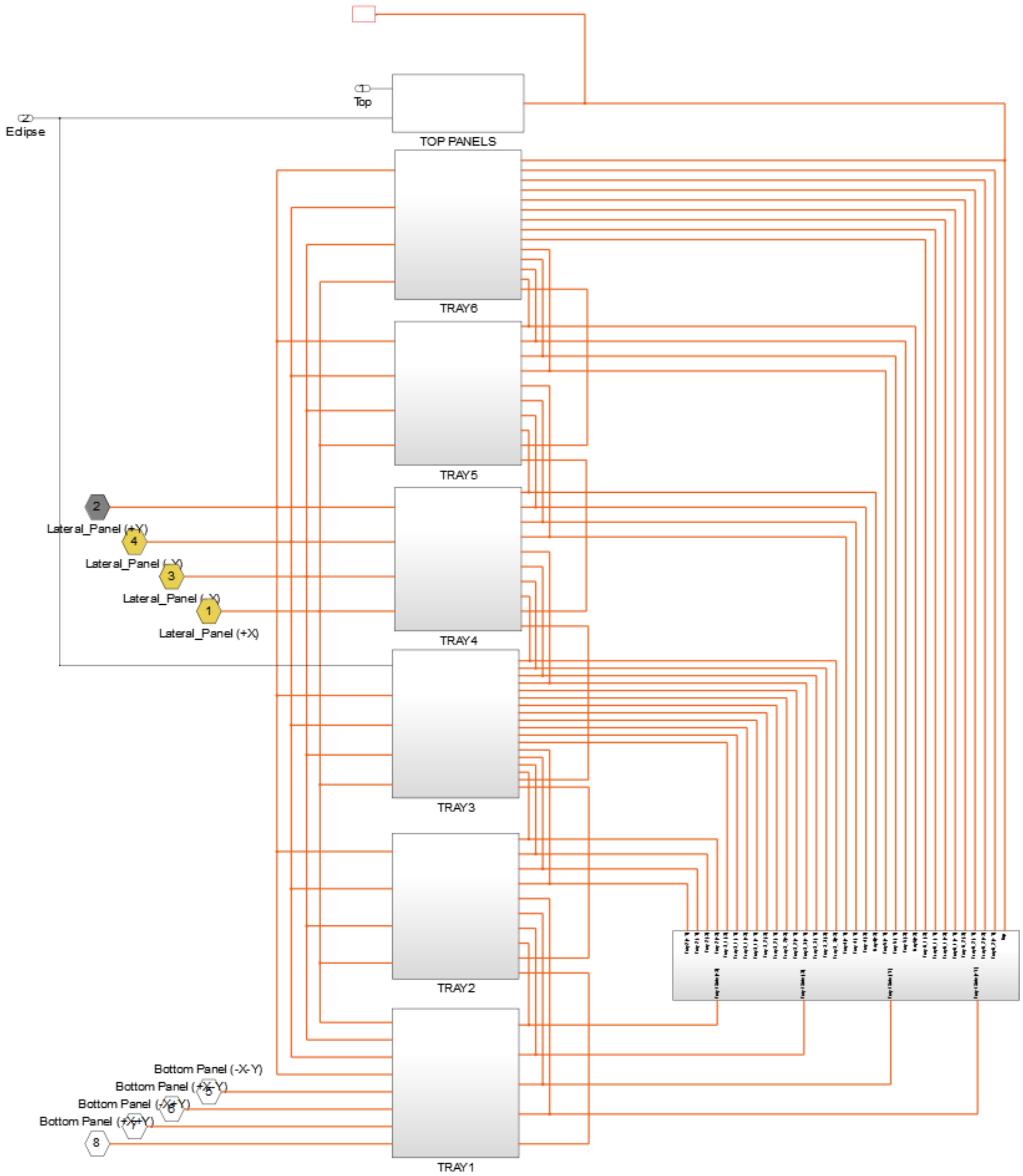

Figure 15: Thermal network of Top panel and BM [14]

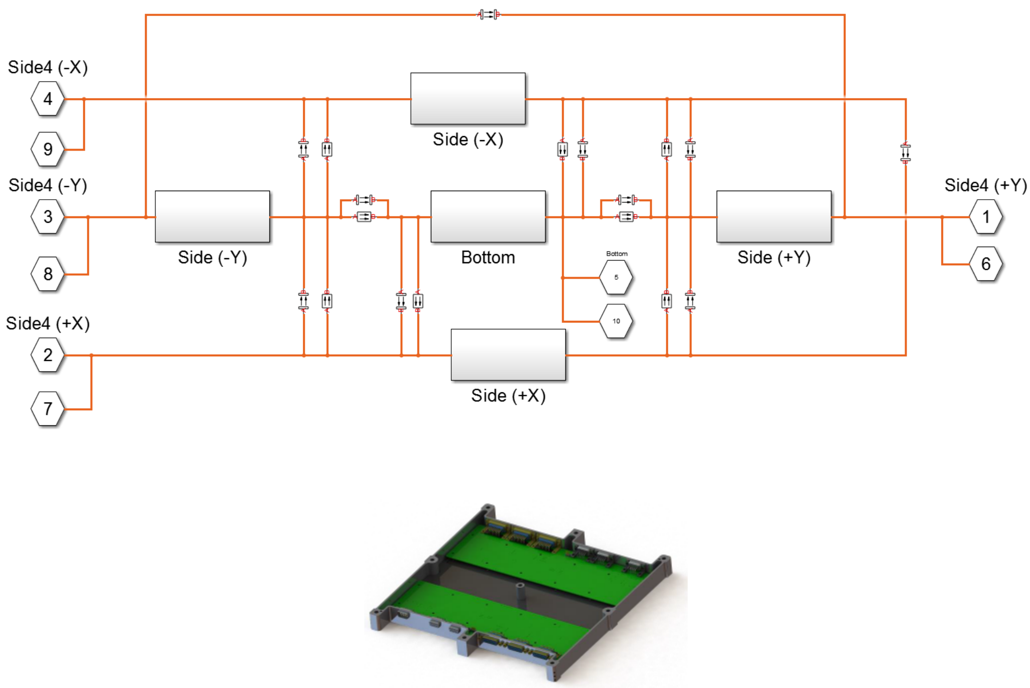

Figure 16: Thermal network of Tray 4 and its final configuration [14]

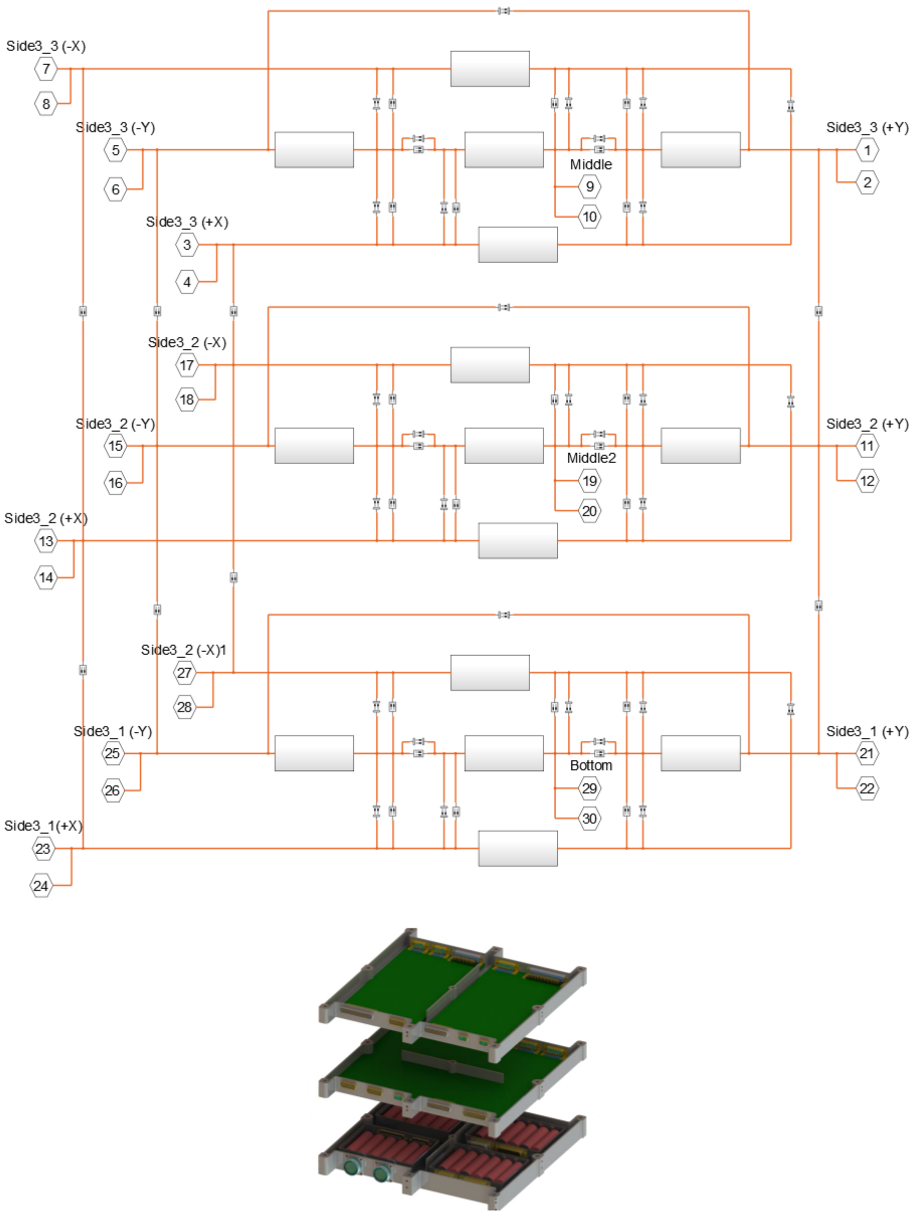

Figure 17: Thermal network of Tray 3 and its final configuration [14]

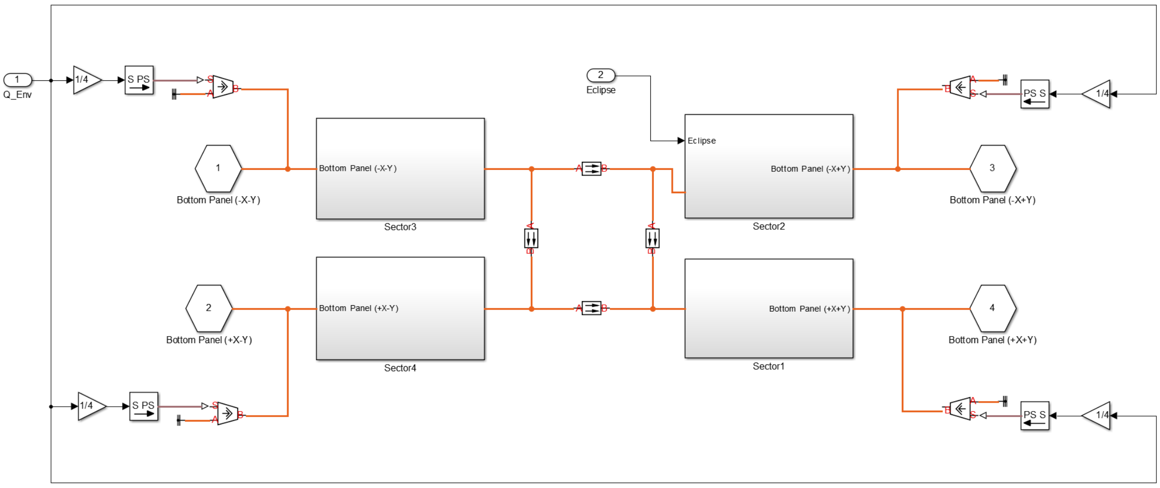

Figure 18: Thermal network of Bottom panel [14]

Payload module

It is composed by a series of four vertical composite panels, a top composite panel (bottom plate of Tray 1), an aluminum bottom plate (Bottom panel) as interface with the launch vehicle adapter and four beams (*Payload Bay Bar*) as mounting supports for lateral panels.
From the thermal network point of view, each Payload Bay Panel (*Location*) represents a node; this is valid for all the vertical panels except for *Payload Bay Panel (+X)* and *Payload Bay Panel (+Y)*, each divided in two nodes (Figure 19).

Lateral panels and payloads

Each lateral panel is composed of two elements, the first one (PM Lateral Panel *Location*) representative of the honeycomb panel supporting the solar cells is modelled with 3 or 4 nodes: one for

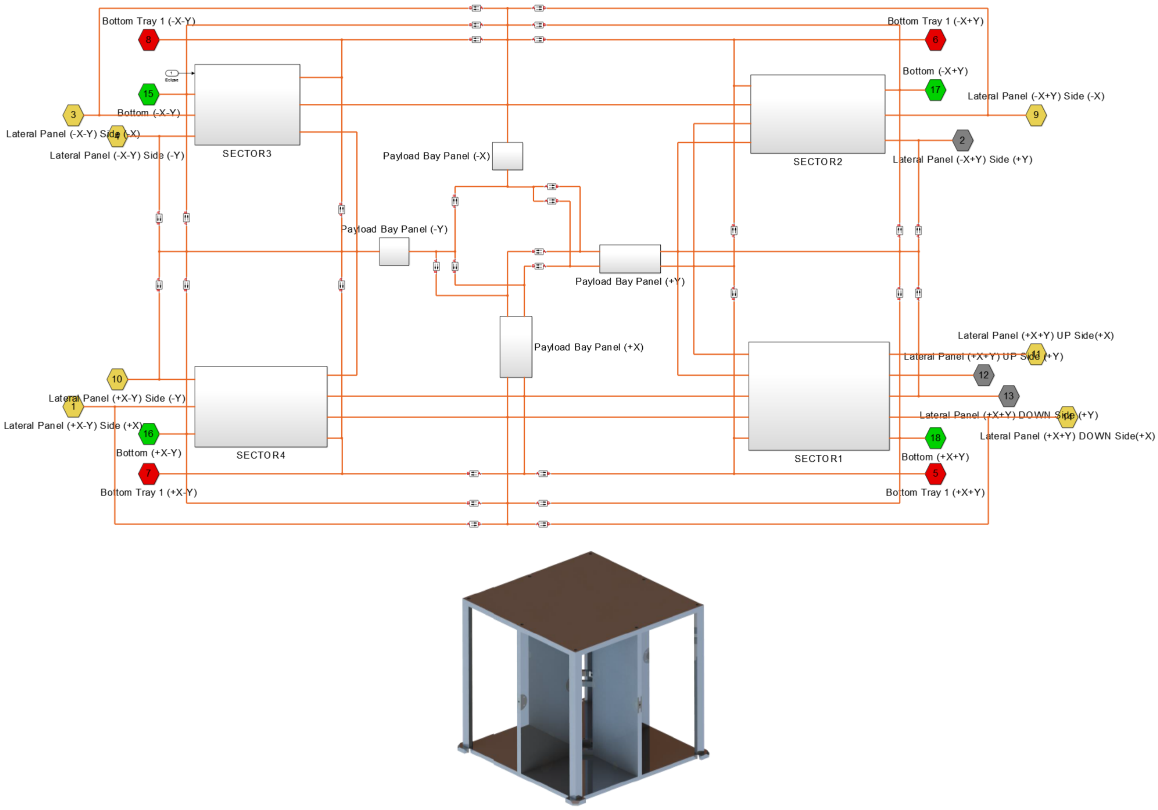

Figure 19: Thermal network of PM and its module structure [14]

the section that covers the BM and one or two for each parts that cover the sectors of the PM; the second one (Solar_Panel (*Location*)) representing the solar cells plus the insulating layers and it is modelled with a single node (Figure 20).
This division is not valid for the lateral panel that works like a radiator (*LateralPanel (+Y)*). It is considered like a single elements, modelled with 4 nodes (Figure 21).
At least each payload is modelled with a single node (*Name of the payload*) and, at this purpose, the modelling of DOM is reported in Figure 21.

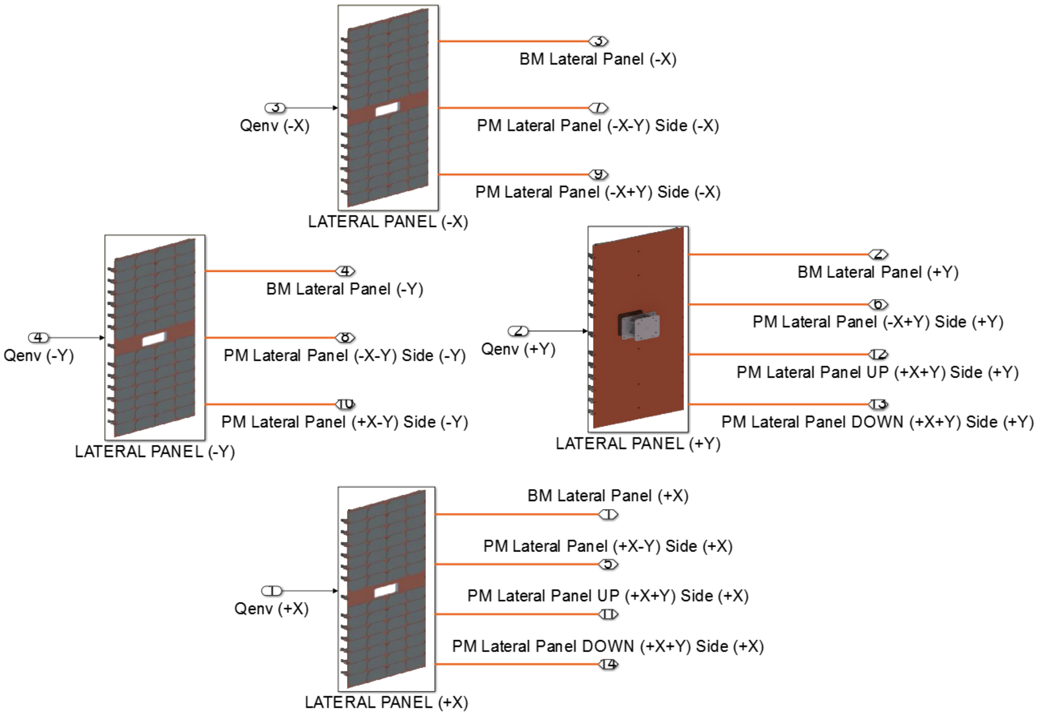

Figure 20: Thermal network of lateral panels

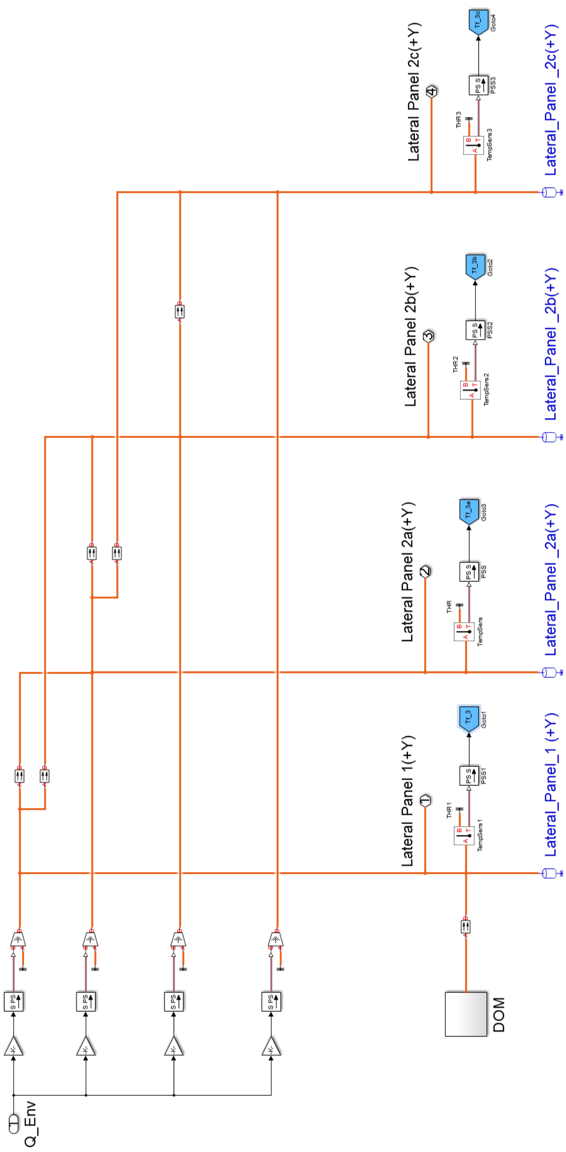

Figure 21: Thermal network of lateral panel (+Y)

6.2.2 Definition of links

This is another important step in order to design a correct thermal model. As reported in Section 6.1.1, a link represents the heat flow path between two nodes and it can be radiative or conductive.

Radiative links

In ESEO thermal network radiative links are impemented relying on the evaluation of the radiative exchange factor with the Gebhart method. Applying this means that all the hypotheses reported in Section 6.1.3 must be valid in our thermal model; in particular the presence of an enclosure is an important constrain. R_{ij} and so B_{ij} can be evaluated according to the matrix equation 6.7 once we know the thermal-optical properties of each surfaces [15] and the view factor among them [13].
In particular the Gebhart Factors can be evaluated according to the following schemes:

- **Radiation inside a tray**
  Modelling the radiative heat transfer among the internal surfaces of a tray is not so complicate because the tray itself represents an enclosure (Figure 22).
  In this case we find a symmetric 6x6 matrix of Gebhart factors for each tray according to the different dimension and thermal-optical properties of the surfaces.
  For the sake of completeness, the previous scheme is not valid for Tray 1 because its bottom plate is divided in four equal parts. In this case the scheme for the calculation of $[B]$ is reported in Figure 23 and it is not hard to recognized that this scheme is equal to the one reported in Section 4.3. Moreover, for the conservation of energy, it is important that the sum of each row is equal to one. This last constrain will be fulfilled in all the following cases.

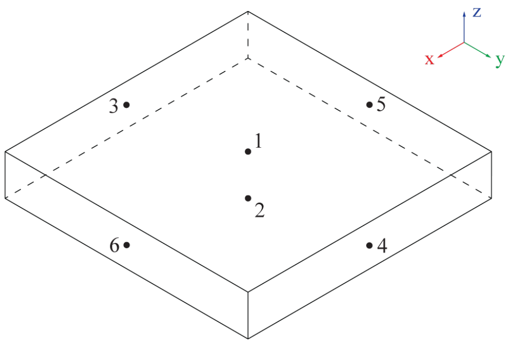

Figure 22: Scheme of nodes of a generic tray

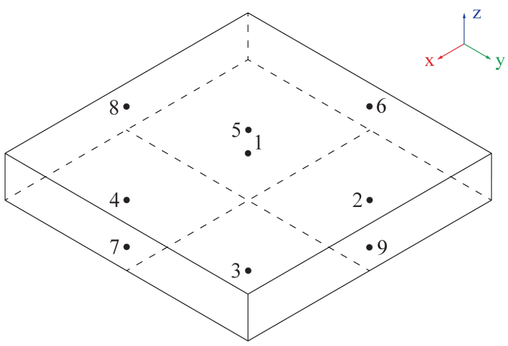

Figure 23: Scheme of nodes of Tray 1

- **Radiation in the Payload module**
  The architecture of the PM (Figure 24) is more complex than the one of the BM and this reflects on a major difficulty in modelling the radiative heat transfers.

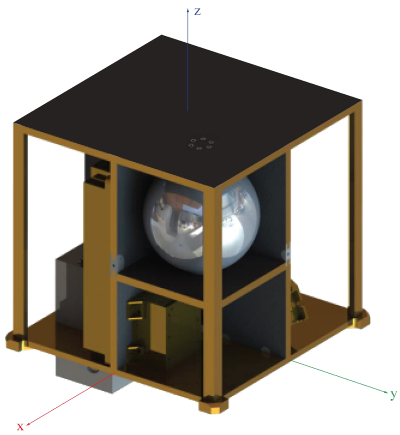

Figure 24: PM architecture [14]

For this, a reasonable compromise was to consider all the payloads like transparent bodies. The MPS tank, installed in the upper part of Sector 1, represents the only exception. Considering always the fact that the Gebhart method is applicable to an enclosure, the sectors of the payload module (together with lateral panels, bottom plate of Tray 1 and Bottom panel) can be modelled as one or more boxes, each with specific dimension and thermal-optical properties.
According to this, a list of the schemes, used in order to find the Gebhart factors, is as follows:

  - **Sector 1 (+X+Y)**: if the implementation of radiative heat transfer in the lower part (lower part of Figure 25) is not so different from the previous case, the upper part of the sector 1 is modelled like a box with a sphere (upper part of Figure 25) in the middle. In this case, the view factors are evaluated according to the approximation reported in [17];

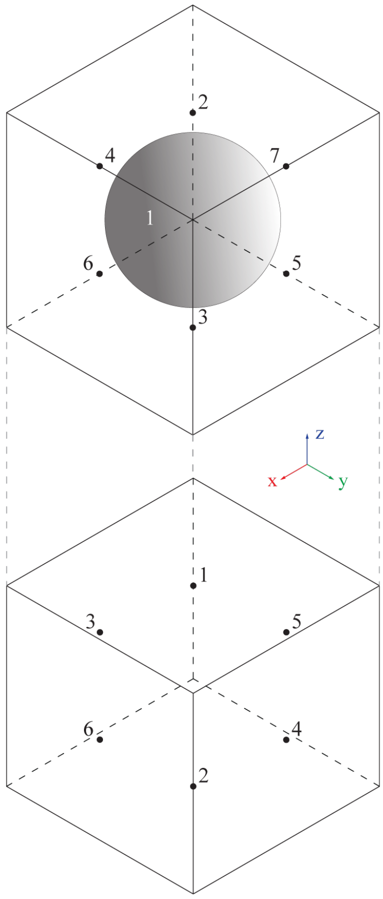

Figure 25: Scheme of Sector 1

– **Sector 2 (-X+Y) and 4 (+X-Y)**: they surround Sector 1 and for this reason the surface in contact with it must me split into two parts (Figure 26). The view factors can be evaluate through the superposition rule (Equation 4.9).

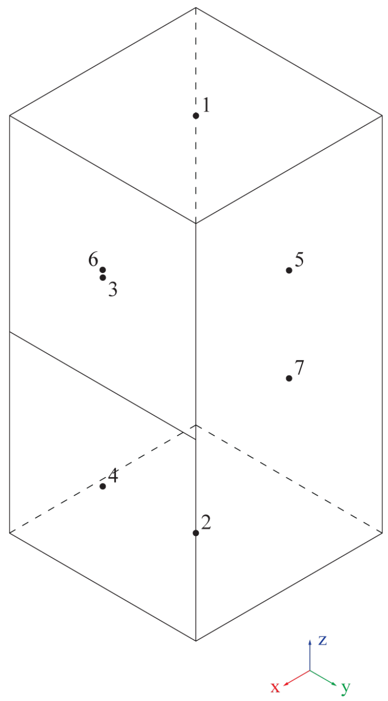

Figure 26: Scheme of Sector 2 and 4

- **Sector 3 (-X-Y)**: it is modelled as a simple box, like the one used to implement the radiative heat transfer inside a tray, but with appropriate dimension and thermal-optical properties. The scheme used to evaluate the matrix of Gebhart factors is reported in Figure 27.

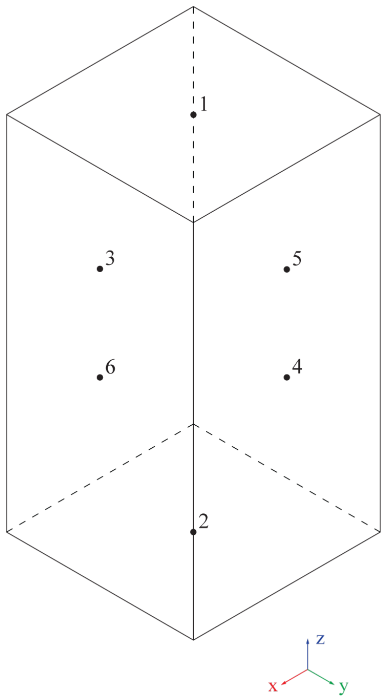

Figure 27: Scheme of Sector 3

- **Radiation Bus module-Lateral panel**
  Fulfilling the hypothesis of enclosure, a lateral panel has been divided in two parts. The first extends over the length of the bus module while the second covers the payload module. Considering the small distance between the lateral panel and sides of the trays it is possible to suppose the interface BM-Lateral panel as an enclosure. The scheme used in the Matlab code is reported in Figure 28.

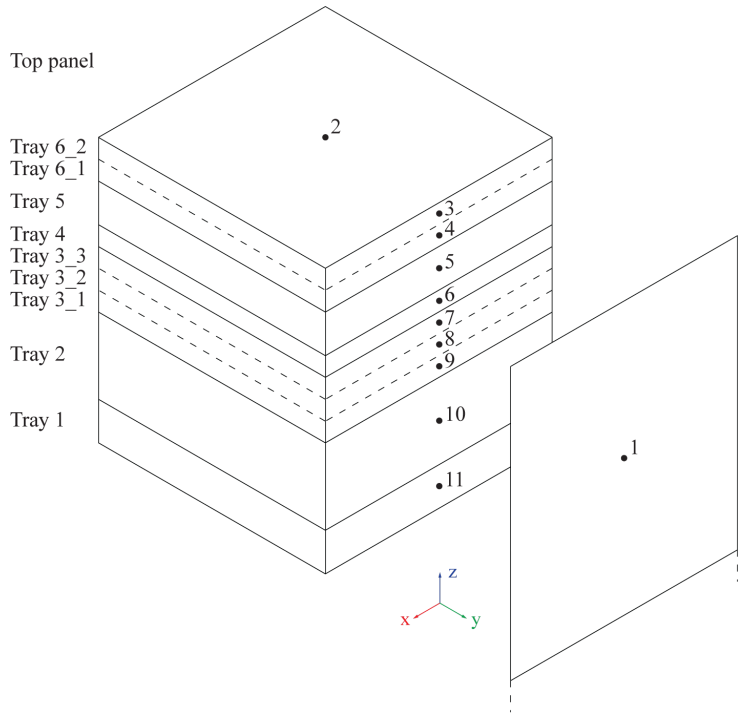

Figure 28: Scheme of BM-Lateral panel interface

Conductive links

According to Section 6.1.1, this type of link is modelled with Equation 6.1. Below is a list of cases used in order to evaluate the appropriate "conduction path", hence, the correct G_{ij} between two generic nodes in the thermal network. To this end, some important parameters like the contact conductances ($Gcont\_n$) and the contact areas are reported in [15].

- **Conduction path between Top panel and Tray 6_2 sides**
  $G4$ is the equivalent conduction between the node that represents Top panel and the one identifies Tray 6_2 (Figure 29);

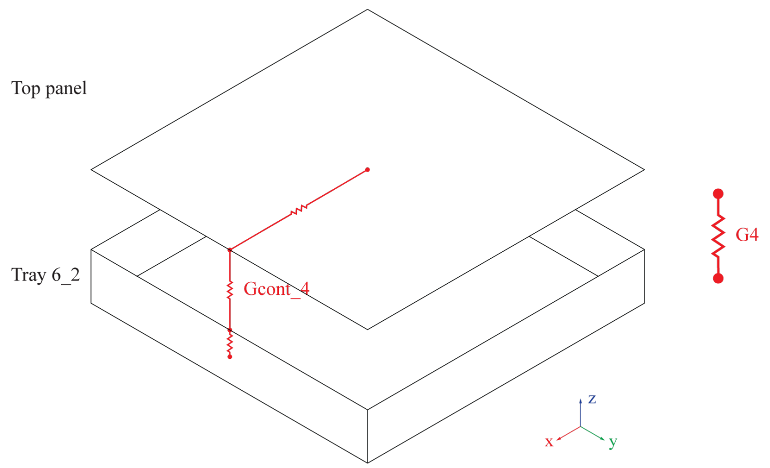

Figure 29: Conduction path between Top panel and Tray 6_2 sides

- **Conduction path inside a tray**
  Considering the choice of the nodes for a tray, it is necessary to take into account the conduction between the four sides.

It is modelled with the equivalent conductance $G3$ (Figure 30).

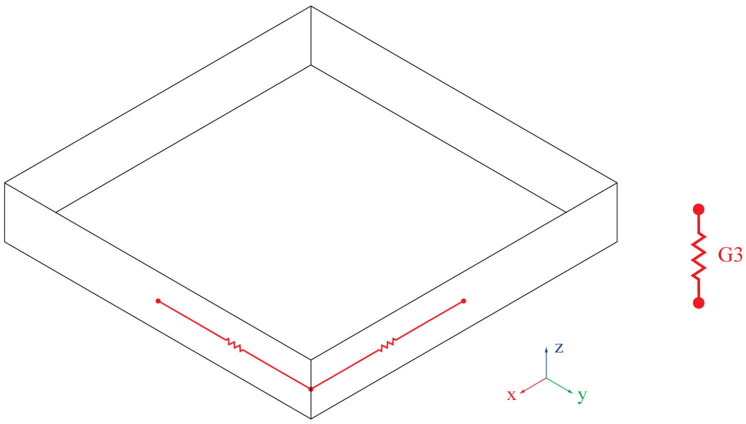

Figure 30: Conduction path between internal sides

Moreover, at the present design status, the tray bottoms are in contact with the same tray frame but not with the rest of trays. According to this, for a generic tray $G2$ is the equivalent conductance between the node of the bottom plate and the node of one side (Figure 31).
This last conductive link is not valid for this tray and $G2$ is replaced by $G10$ (Figure 32).
In this case, since the bottom plate of Tray 1 is divided in four parts, it is necessary to take into account also the conduction between them (Figure 33).
However the scheme reported in the last figure is also valid in the Bottom panel;

- **Conduction path between trays**
  $G1$ represents the equivalent conduction between sides of adjacent trays (Figure 34)and it has different values according to the type of configuration in contact;

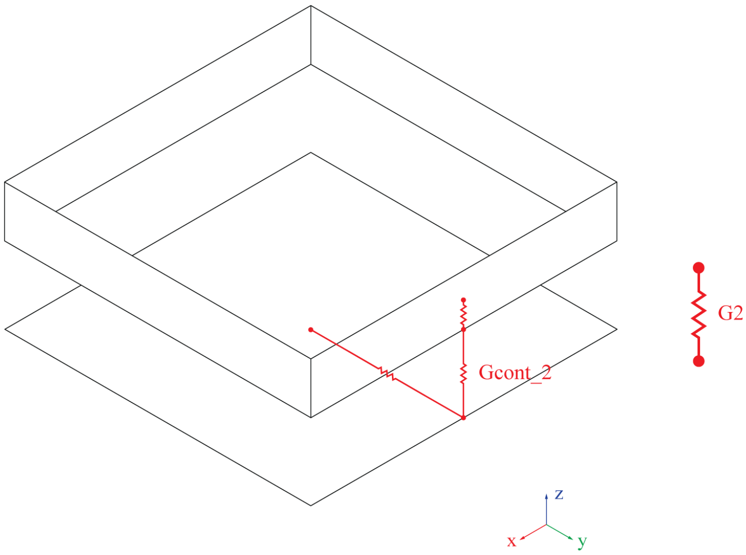

Figure 31: Conduction path between Bottom plate and tray side

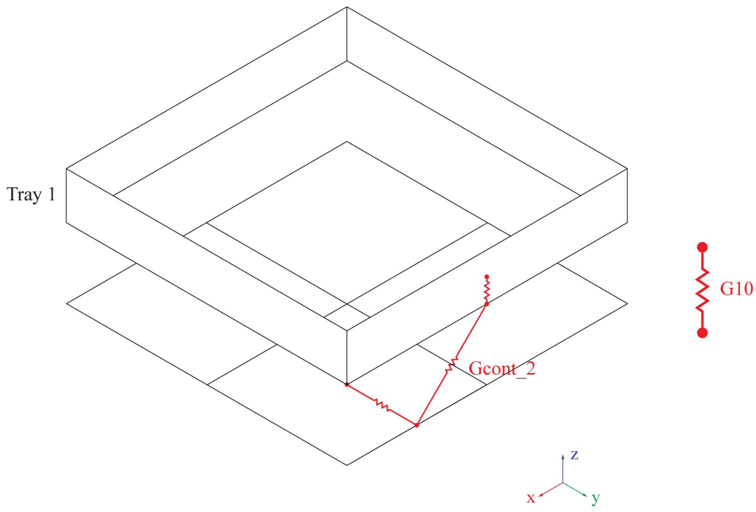

Figure 32: Conduction path between bottom Tray 1 and tray side

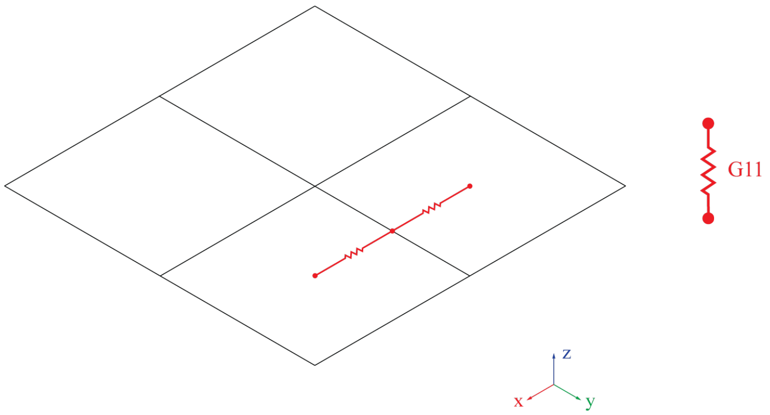

Figure 33: Conduction path in the bottom plate of tray 1

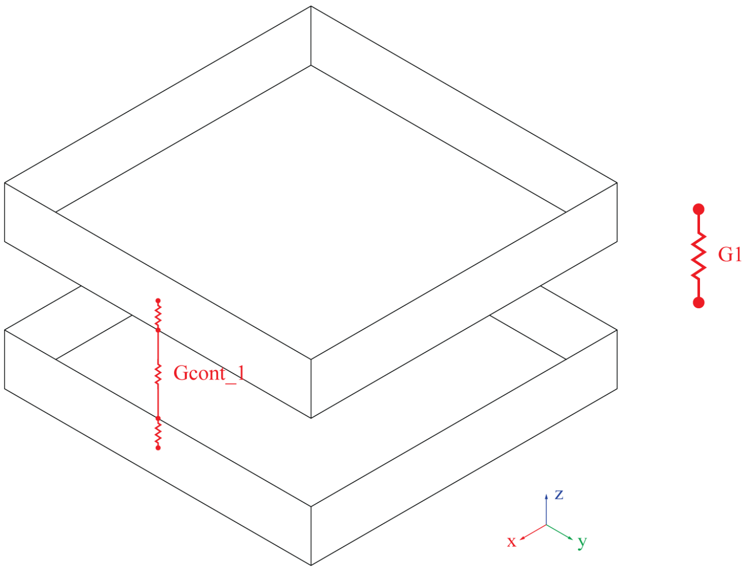

Figure 34: Conduction path between adjacent trays

- **Conduction path inside a lateral panel**
  Because of the discretization used in a lateral panel, it is necessary to take into account the conductive links between the internal nodes. In Figure 35 are reported the equivalent conductances for all the possible cases, according to the location of the lateral panel;

- **Conduction path between lateral panels and spacecraft structure**
  The contact between lateral panels and spacecraft structure is guaranteed by means of spacers and angular elements (Figure 36).
  The first, modelled as a conductance (*Gang*), have been linked to sides of trays 1, 3 and 6 (Figure 37-upper part) and to the Payload bay bar; in particular, this last case is included in the conduction path between lateral panels and the Bottom panel (Figure 37-lower part). Located on the right of each scheme, there are the equivalent conductances considered in the Simscape model.
  The second (*Gsp*) have been linked to the Bottom panel and to trays 1, 3 and 6 (Figure 38). In this situation, the equivalent conductances are $G7$.

- **Conduction path between the bottom plate of Tray 1 and Payload bay panels**
  The conductive link between the bottom plate of Tray 1 and Payload bay panels is modelled with the parameter $G12$ (Figure 39) and, according to which Payload bay panel we are considering, we have different values of it.

- **Conduction path between Payload bay panels and Bottom panel**
  In an analogous way at the previous case, $G13$ represents

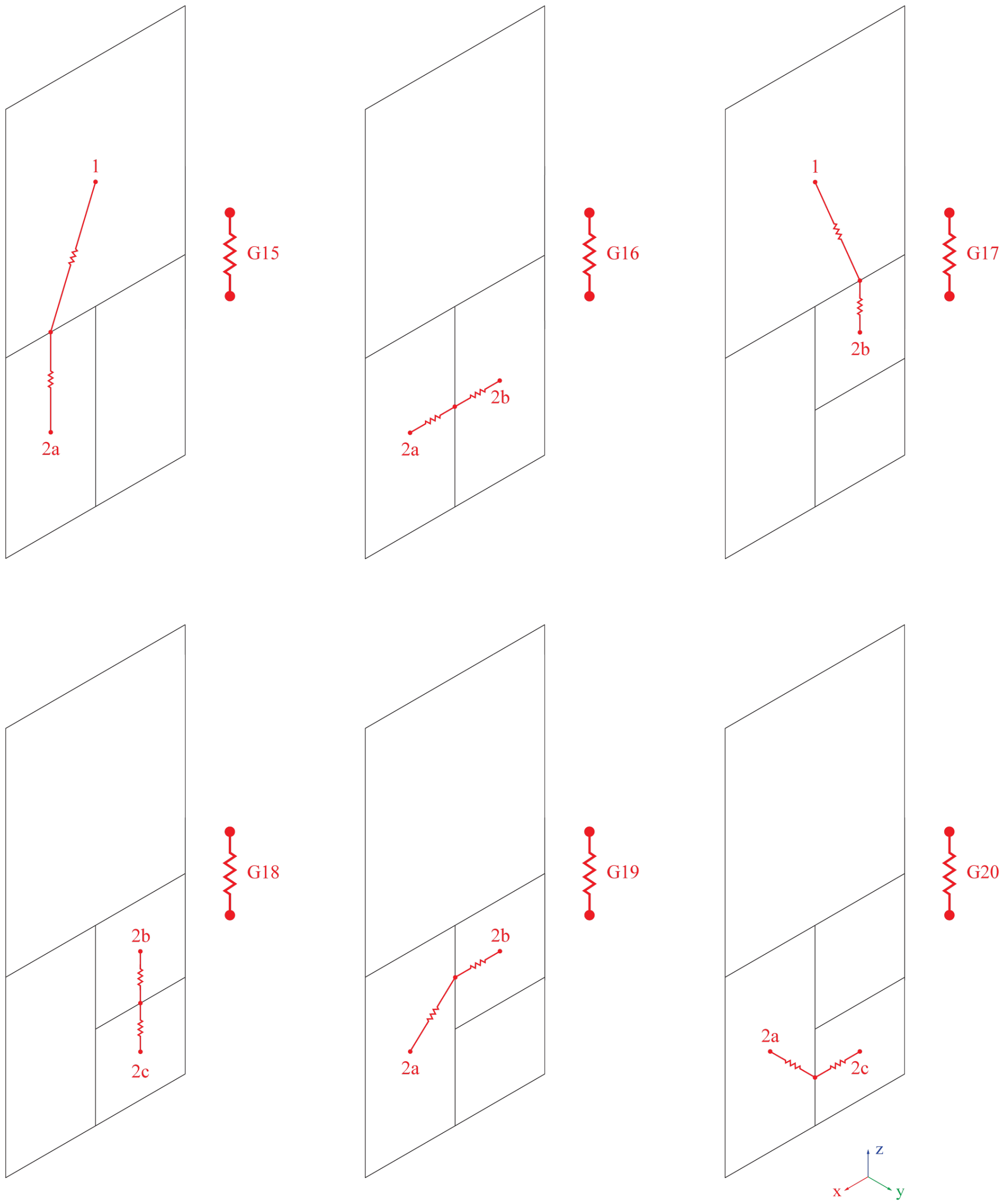

Figure 35: Conduction paths insides a lateral panel

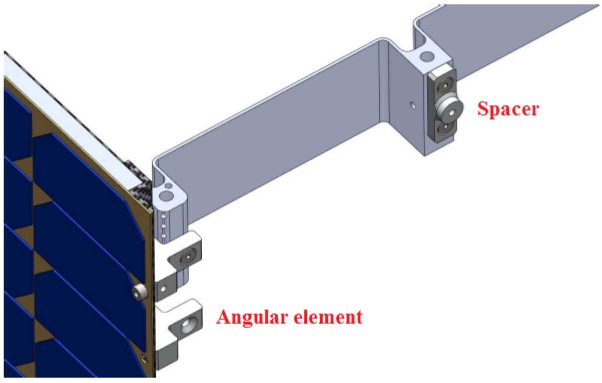

Figure 36: Lateral panel mounting concept [14]

the equivalent conductance between Payloads bay panels and Bottom panel (Figure 40).

- **Conduction path between bottom plate of Tray 1 and Bottom panel**
  The conduction path between bottom plate of Tray 1 and Bottom panel is characterized by the presence of four beams. From the thermal network point of view these are not nodes and they are considered with appropriate conductance (Figure 41) and the parameter to take into account in order to model this conductive link is $G9$;

- **Conduction path among Payloads bay panels**
  Considering the different discretization, used for the Payload bay panels, we have different conductive paths according to the location of each node. Moreover, although the different conductance values, in the Simscape model these are characterized by the parameter $G14$ and in particular two cases are reported in Figure 42.

- **Conduction path among Payloads bay panels**

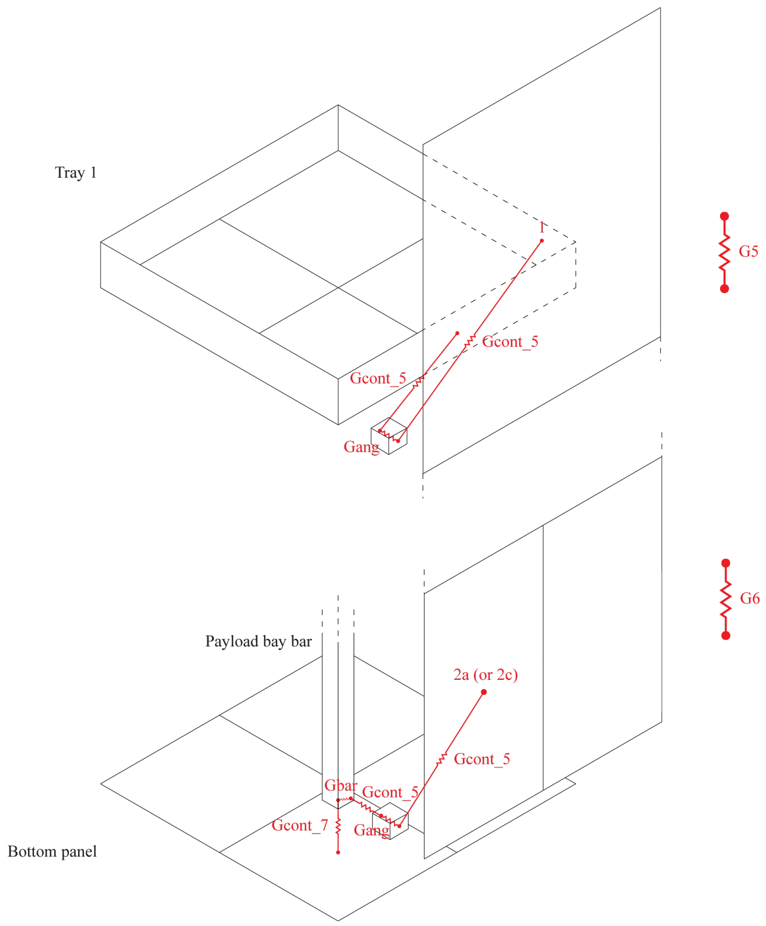

Figure 37: Conduction path with angular elements

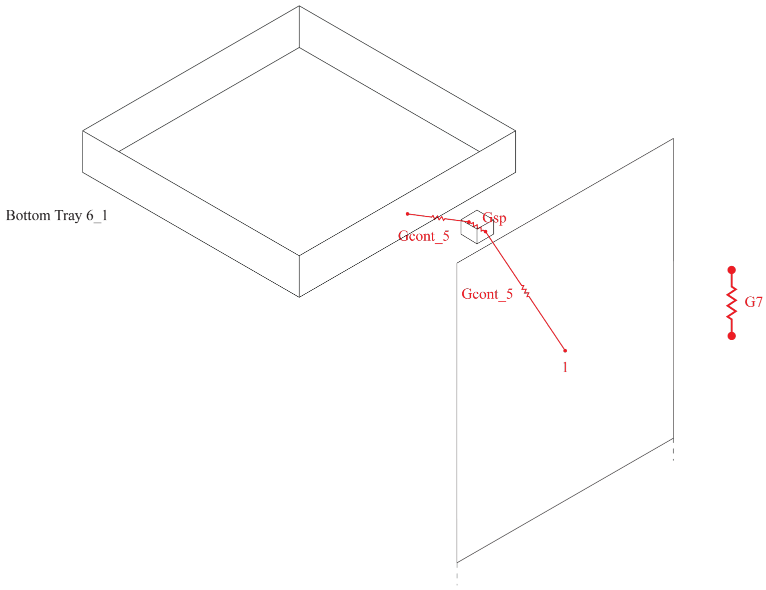

Figure 38: Conduction path with spacers

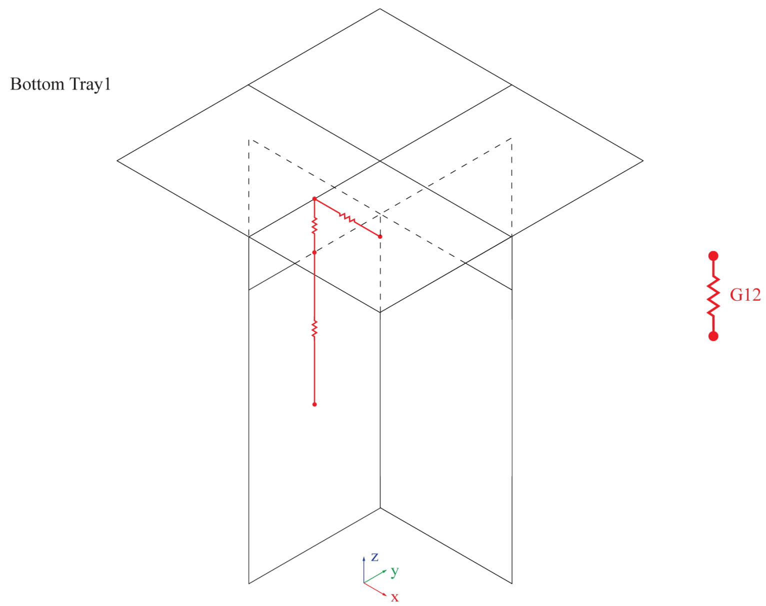

Figure 39: Conduction path between the bottom plate of Tray 1 and Payload bay panels

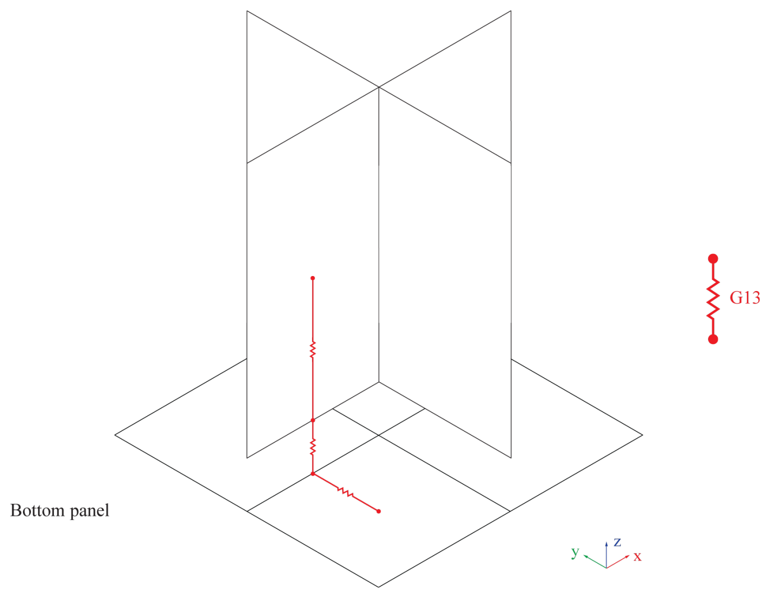

Figure 40: Conduction path between Payload bay panels and Bottom panel

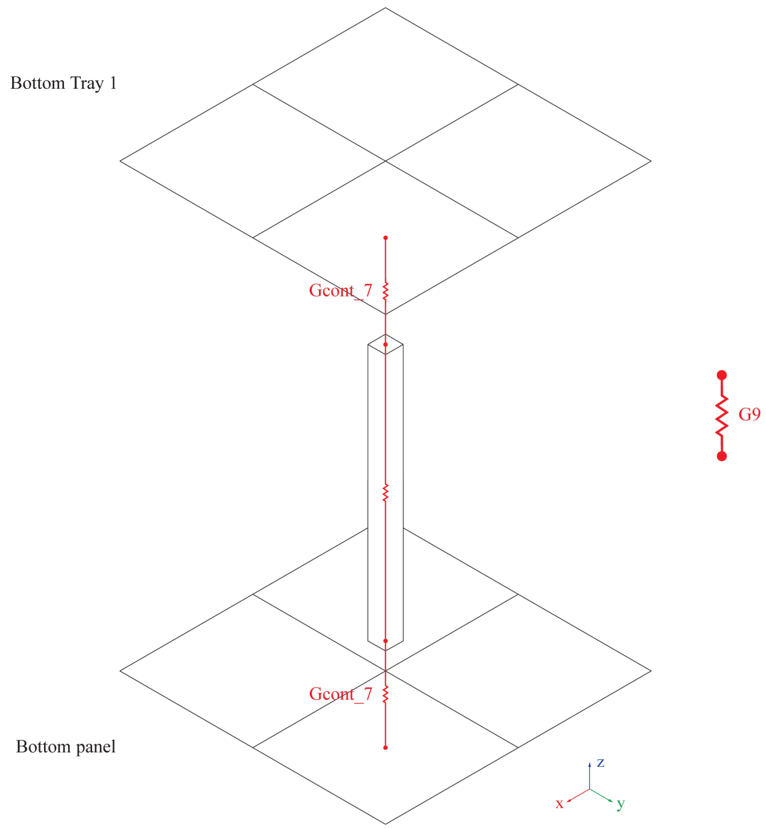

Figure 41: Conduction path between bottom plate of Tray 1 and Bottom panel

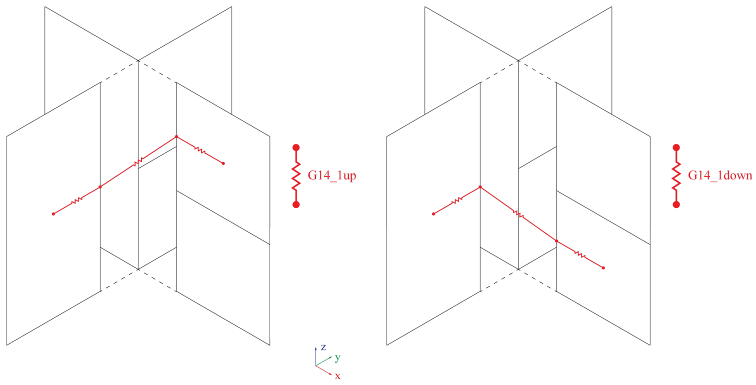

Figure 42: Conduction path among Payload bay panels

The Payload bay Panel (+Y) (and also (+X)) is modelled with two nodes and so it is necessary to consider the conduction between them (Figure 43).

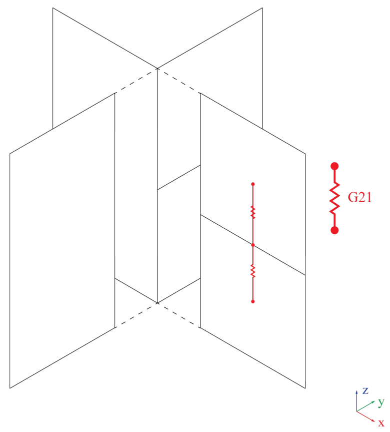

Figure 43: Conduction path inside Payload Bay panel

6.3 ESEO thermal model validation

The final step is to verify the accuracy of our work. In order to do this we have to compare our results with those provided by the Prime Contractor SITAEL using ESATAN under two critical mission scenarios in terms of Earth-Sun distance and solar activities:

- **Case A**: ESEO nominal orbit at 08/03/2016 with J=1397$\frac{W}{m^2}$ =cost
- **Case B**: ESEO nominal orbit at 29/07/2016 with J=1426$\frac{W}{m^2}$ =cost

In particular the first produces the minimum ESEO platform operating temperatures while the second the maximum one.
For a correct comparison of the results it is necessary to replicate the exact boundary conditions not only in terms of orbit and environmental parameters but also considering the power transmitted from the units to the satellite.

6.3.1 Orbit and environmental parameters

The orbit parameters as so as the Sun position have been identified in the thermal design report by means of the SDK suite and are reported in Table 3.

6.3.2 Power of units

As we have already mentioned, case A produces the minimum value of temperatures and so the thermal analysis has been defined for *cold* configuration of the ESEO mission. In this case the spacecraft is operating in *power safe mode* with only vital units switched on, according to the mission needings.
The maximum temperatures are reached for the case B where the satellite is operating in nominal conditions with all unites switched

	CASE A	**CASE B**
Orbit parameters		
Altitude of Apogee	536.135 km	536.135 km
Altitude of Perigee	517.519 km	517.519 km
Inclination	97.479°	97.479°
RAAN	322.899°	102.314°
Argument of Perigee	135.309°	5.122°
Environment parameters		
Sun-Earth distance	148492215.240 km	151904564.970 km
Solar declination	−4.892°	18.988°
Sun's RAAN	127.476°	127.476°

Table 3: Orbit and environmental parameters [15]

on, according to the mission needings.
In Table 4 is reported all the power transmitted from the units to the satellite, in both cases.
For the sake of completeness the unknown acronyms reported in the first column of Table 4 stand for:

- LNA: Low Noise Amplifier;
- MTM: Printed circuits board of MagnetoMeter (MM);
- MTC: Printed circuit board of MagnetoTorque (MT);
- PDU: Power Distribution Unit;
- PMB: Power Management Board;
- RTX: Receiver & Transmitter;
- HPA: High-Power Amplifier.

POWER OF UNITS			
	CASE A	**CASE B**	
Unit	**Value [W]**		**Remarks**
OBDH	1.1	1.1	
ES	0	2.16	In eclipse only
HSTX	0	12	10 minutes of duration per orbit, in sunlight only
LNA	2×0.2	2×0.2	
MTM	0	1.1	
MM	0	0.95	
MTC	0	2×0.6	
MT	0	4×0.31	
MW	0	1.2144	
PDU	2×1.2	2×1.2	
PMB	2×1.485	2×1.485	
RTX	4×1.95	4×1.95	2 seconds duration, periodically after 5 minutes
HPA	7.70	7.70	2 seconds duration, periodically after 5 minutes
SS	0	2×0.66	In sunlight only
BPs	6×0.005	6×0.005	In eclipse only

Table 4: Power of units [15]

The contribution of the units working only in sunlight (SS) or in eclipse (BPs and ES) has been implemented in the thermal model only with a *switch block* while, in addiction, a *pulse generator block* (opportunely enabled) must be taken into account in order to model the periodical contribution of the RTX, HPA and HSTX. As an example, the Simulink block that implements the power consumption of the HSTXis reported in Figure 44. In particular the constant signal *case_flag* can be 1 (hot case) or 0 (cold case) in order to enable or disable, respectively, a particular unit.

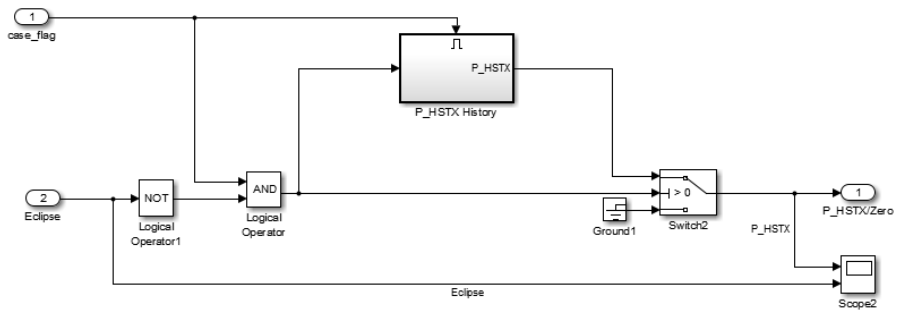

Figure 44: HSTX Activity

6.3.3 Comparing the results

For a correct thermal analysis, an important point is to consider the proper environmental fluxes.
According to this, the environmental fluxes that every surface of the satellite receives, during an orbit, are reported from Figure 45 to 50.

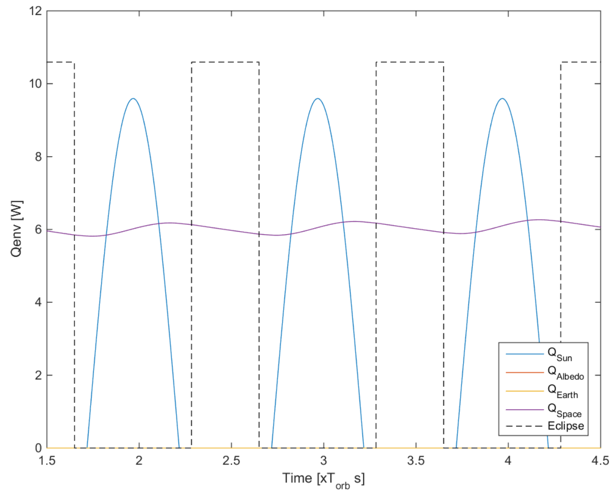

Figure 45: Environmental flux on Top panel

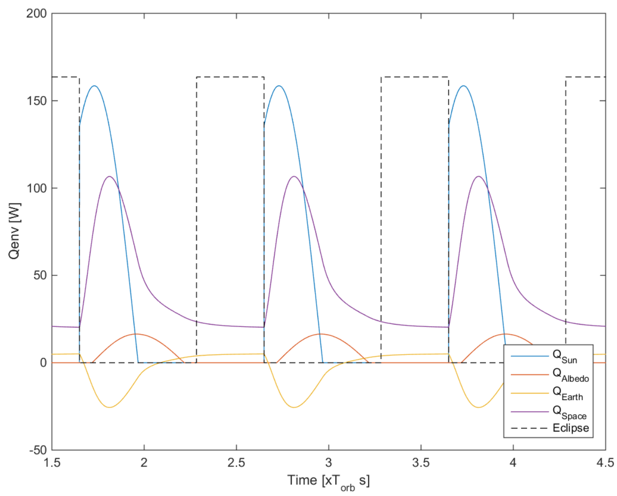

Figure 46: Environmental flux on Lateral panel (+X)

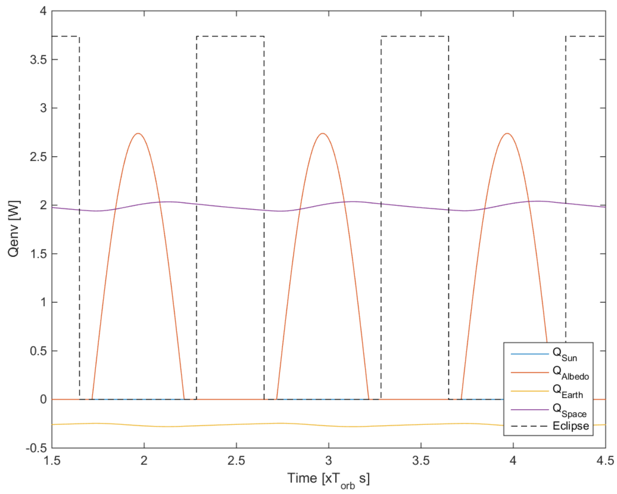

Figure 47: Environmental flux on Lateral panel (+Y)

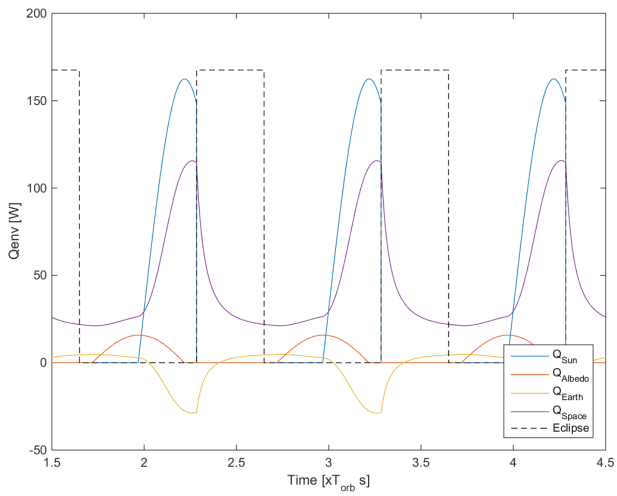

Figure 48: Environmental flux on Lateral panel (-X)

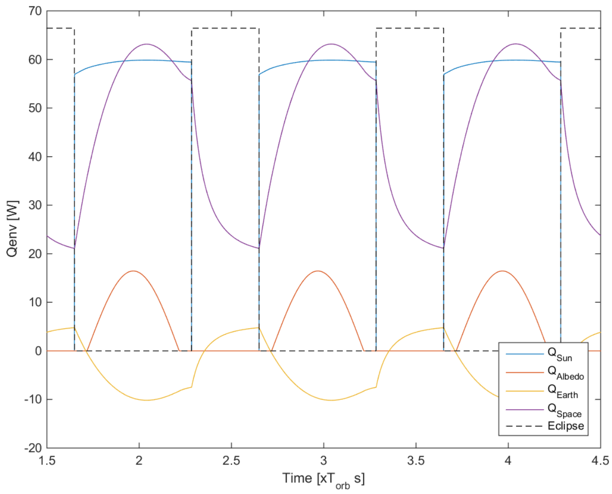

Figure 49: Environmental flux on Lateral panel (-Y)

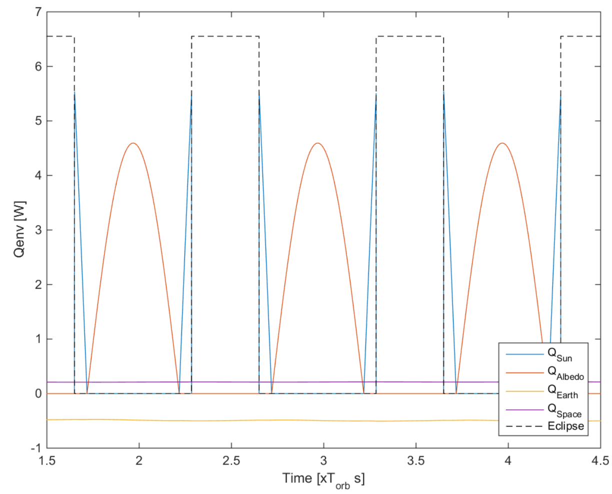

Figure 50: Environmental flux on Bottom panel

It is evident as the Top panel (Figure 45) is affected only by the incoming solar radiation and by a negative flux through deep space. At the same time, in the opposite side, the Bottom panel (Figure 56) receives the radiation from the Sun only at the beginning and at the end of the sunlight mode. Moreover from Figure 47, the design choice to remove solar cells and to consider the lateral panel (+Y) as radiator, is justified.
The following step in the validation phase is the analysis of the accuracy of the external panel temperatures. From Figure 51 to 56 we have a comparison between our results and those computed with ESATAN in the hot case.
However, it is important to point out that the initial transient reported in the following figures is due to the choice of the initial temperature of the thermal network nodes. For a correct analysis, the final part of plots (when the transient is over) must be taken into account.

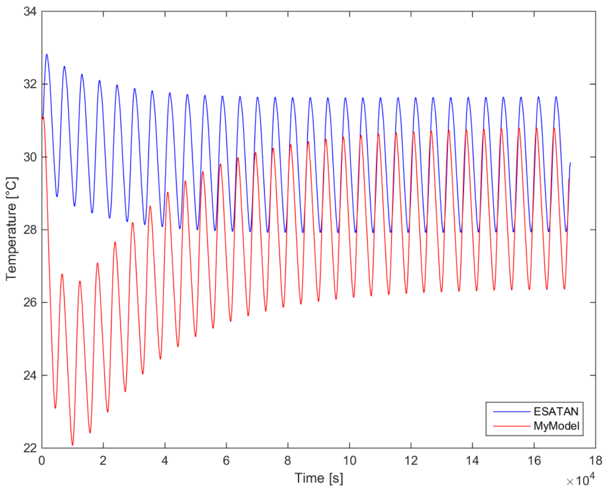

Figure 51: Temperature of Top panel

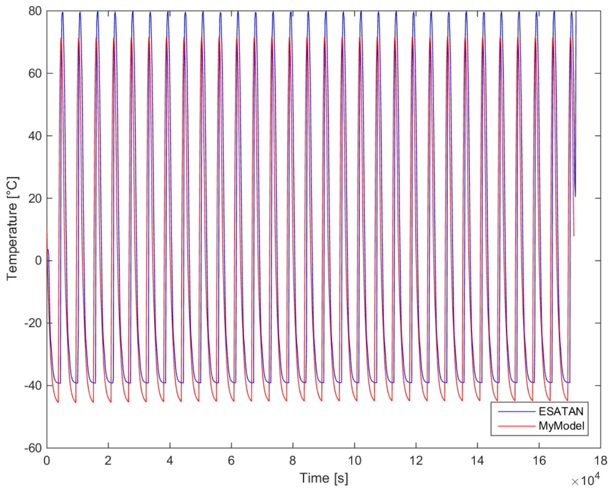

Figure 52: Temperature of Lateral panel (+X)

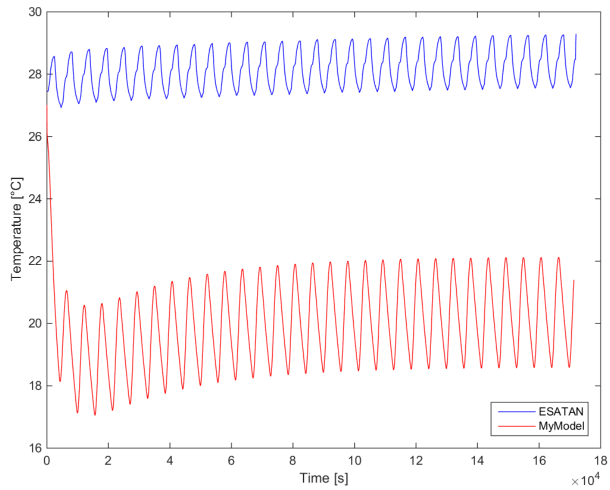

Figure 53: Temperature of Lateral panel (+Y)

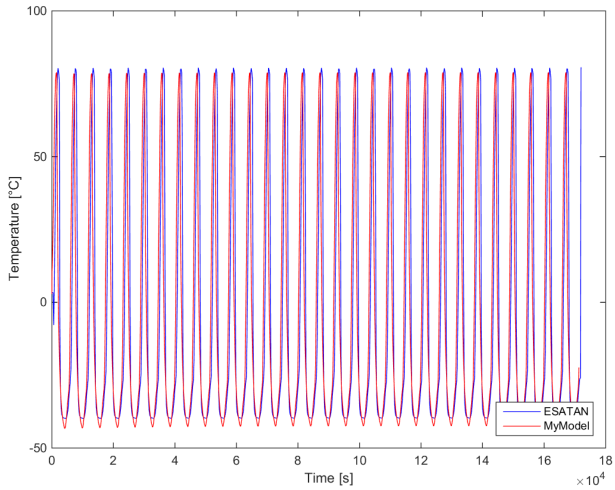

Figure 54: Temperature of Lateral panel (-X)

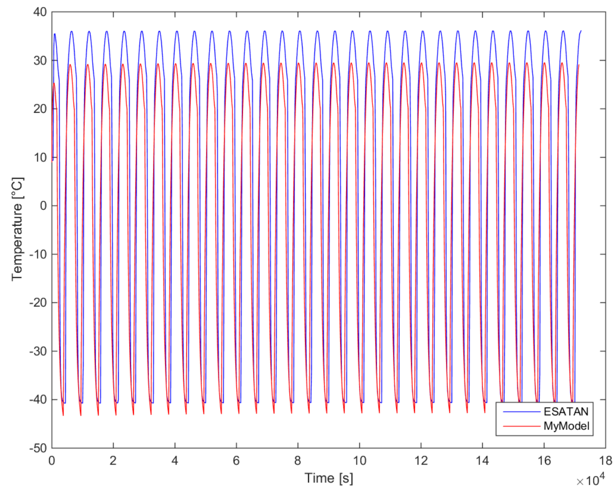

Figure 55: Temperature of Lateral panel (-Y)

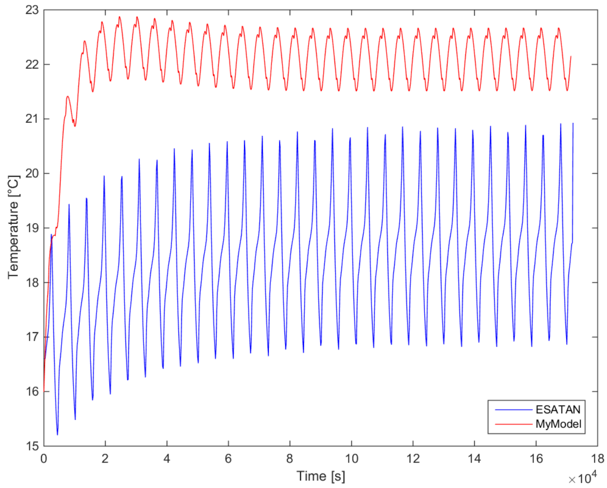

Figure 56: Temperature of Bottom panel

The analysis, made with ESATAN, has been performed on a minimum number of orbits (30), necessary to reach convergence in the results. Moreover a $\pm 10°C$ uncertainty margin has been applied on the minimum and maximum estimated values ($\pm 15°C$ for the units mounted outside the spacecraft). About the lateral panel in the y-direction (Figure 53) and the Bottom panel (Figure 56), a greater gap is related to the important, but inevitable, approximation made in modelling payloads and subsystems, especially in the PM.
The final step in the validation phase concerns the analysis of the temperature of some elements contained in the trays of the BM and in the sectors of the PM. From Figure 57 to 68 are reported the values computed with our simulator while, in the Table 5, a comparison with results ESATAN thermal model are made.

	ESATAN model [$^{\circ}C$]	**Our thermal model** [$^{\circ}C$]	**Absolute error**
AMSAT Antenna	33.35	30.80	+2.55
AMSAT Box	21.69	17.28	+4.41
BPs	34.60	25.67	+8.93
DOM	27.41	24.26	+3.15
ES	28.59	31.19	-2.6
GPS Antenna	28.84	30.80	-1.96
GPS Box	41.31	45.28	-3.97
HPA	38.47	34.24	+4.23
HSTX Box	31.86	28.71	+3.15
HSTX Antenna	19.45	22.26	-2.81
LNA	38.50	34.24	+4.26
MM	48.80	45.28	+3.52
OBDH	42.93	42.45	+0.48
PDU	49.03	42.35	+7.58
PMB	48.59	38.72	+9.87
RTX	53.28	46.72	+6.56
SS	33.15	30.80	+2.35

Table 5: Comparison of ESEO platform maximum operating temperatures as predicted by ESATAN model (2nd column) [15] and Simscape model (3rd column)

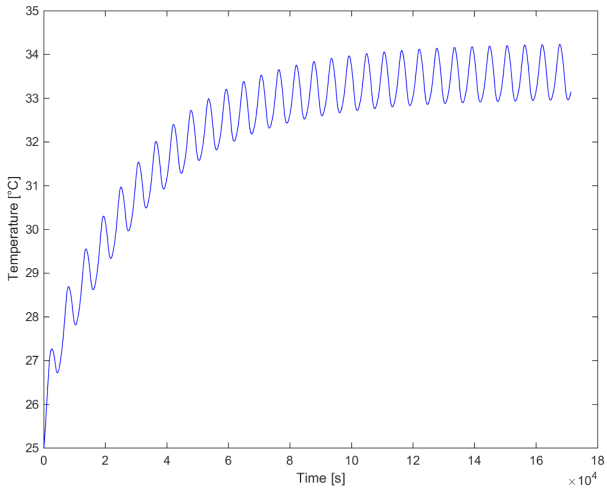

Figure 57: Temperature of Tray 6_2 bottom

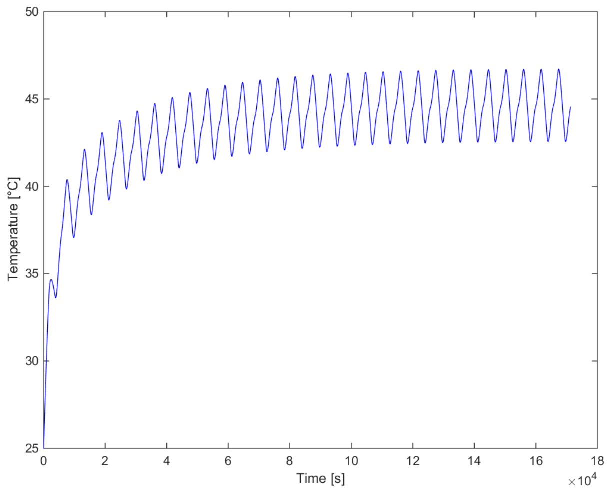

Figure 58: Temperature of Tray 6_1 bottom

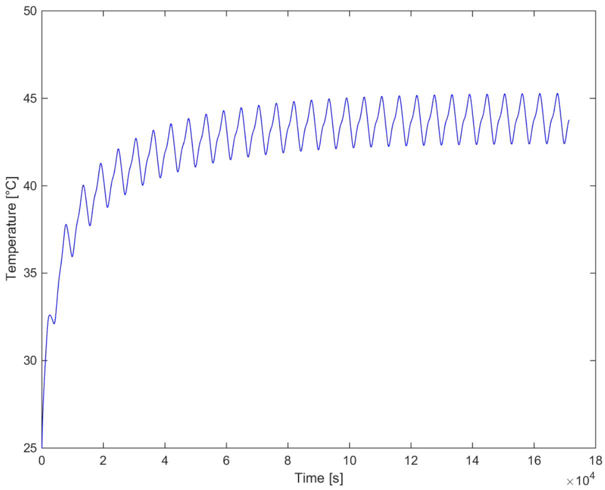

Figure 59: Temperature of Tray 5 bottom

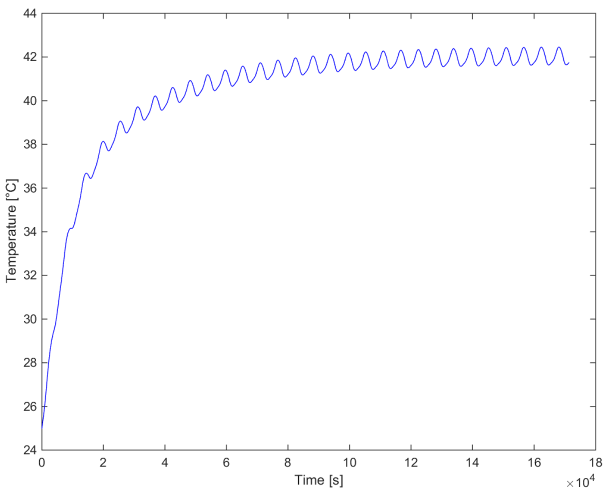

Figure 60: Temperature of Tray 4 bottom

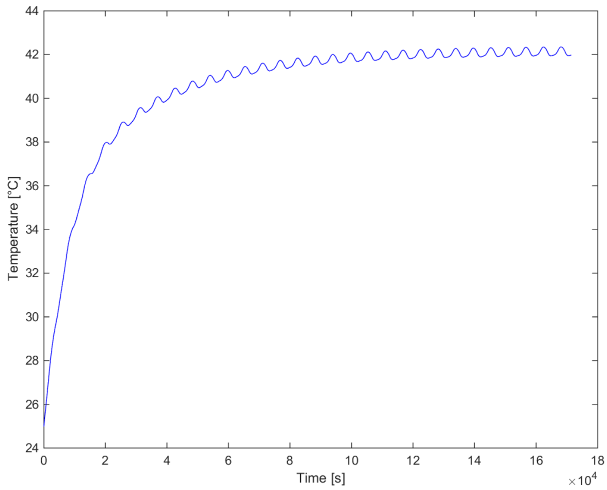

Figure 61: Temperature of Tray 3_3 bottom

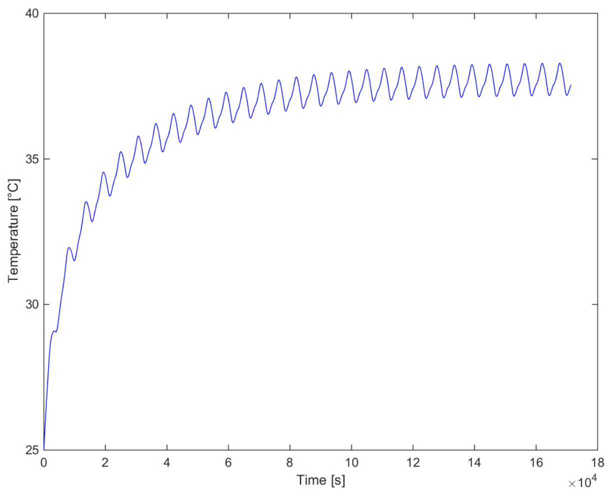

Figure 62: Temperature of Tray 3_2 bottom

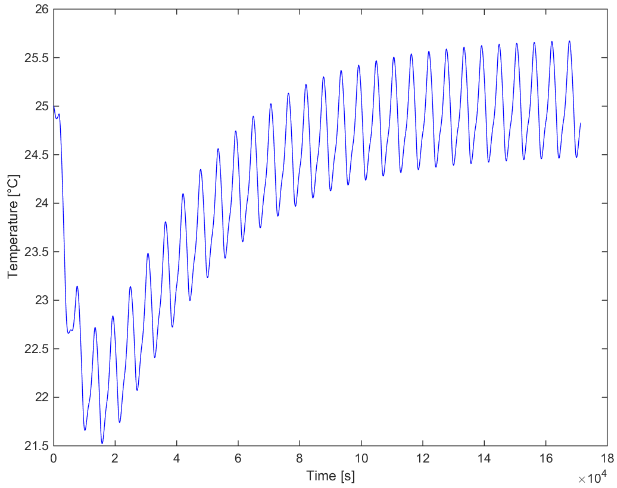

Figure 63: Temperature of Tray 3_1 bottom

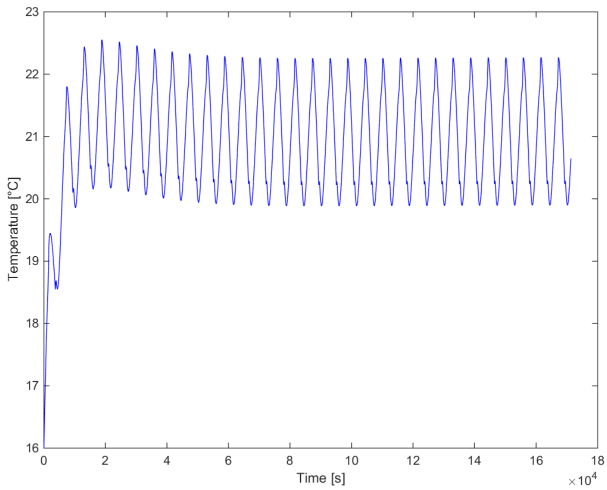

Figure 64: Temperature of Sector 3 bottom

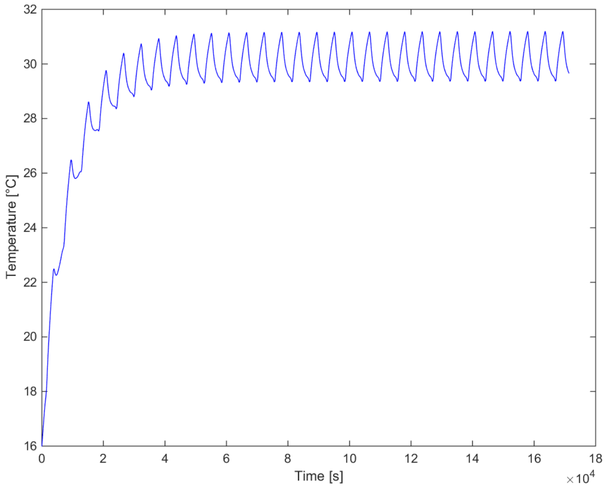

Figure 65: Temperature of Sector 2 bottom

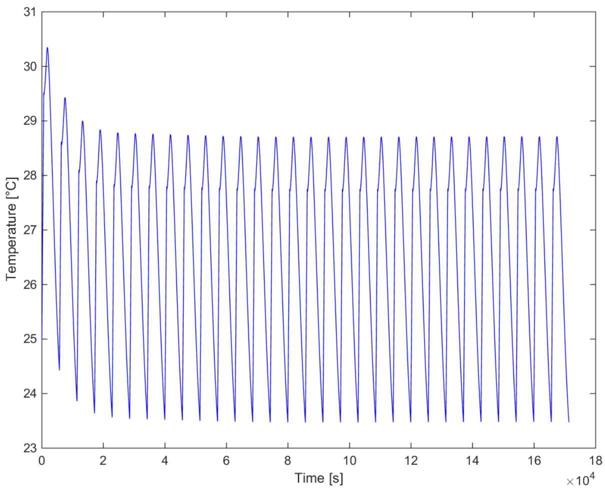

Figure 66: Temperature of HSTX

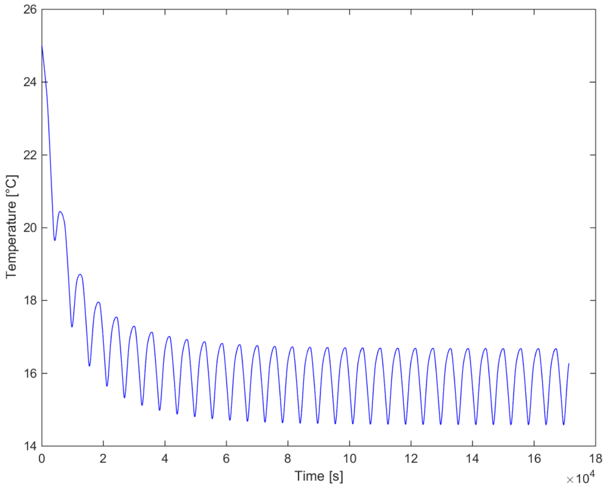

Figure 67: Temperature of AMSAT

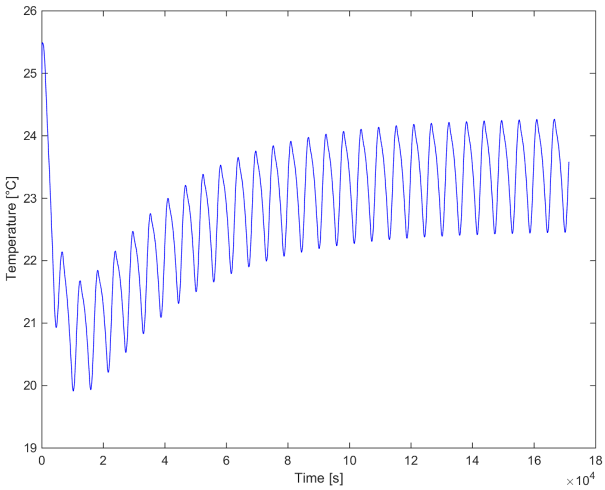

Figure 68: Temperature of DOM

Considering the approximation in modelling of the Payloads Module and that every units temperature of a specific tray are equal to those of the bottom plate, the fact that all the units have a difference considerable lower than the ESATAN uncertainty margin, is considered a good result.
For the sake of completeness, the thermal model outputs for mission scenario A are reported in the following figures. In particular Figure 69 to 74 depict the external panels temperature while Figure 75 to 86 depict ESEO platform operating temperatures at some selected nodes.

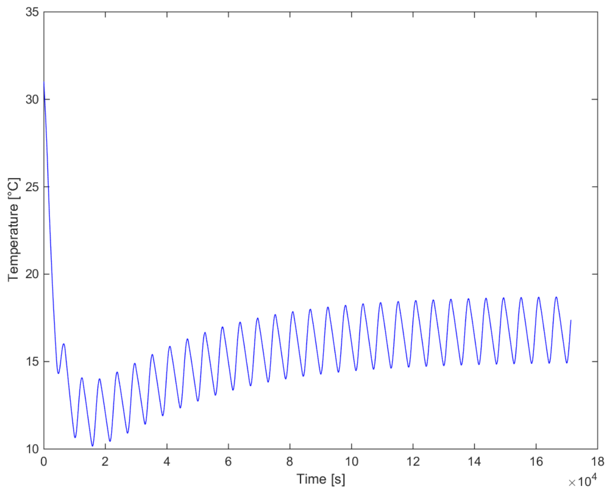

Figure 69: Temperature of Top panel

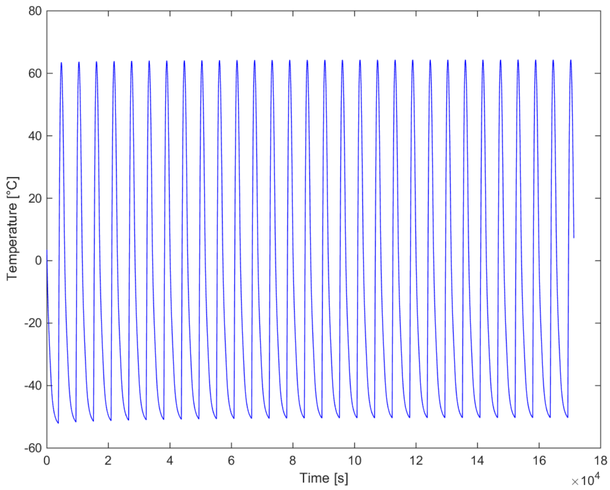

Figure 70: Temperature of Lateral panel (+X)

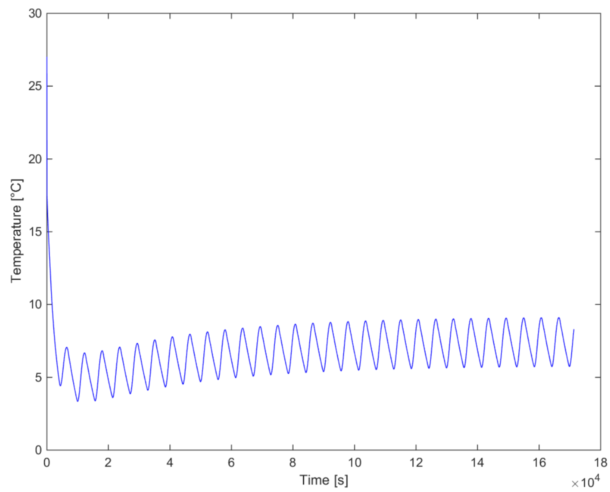

Figure 71: Temperature of Lateral panel (+Y)

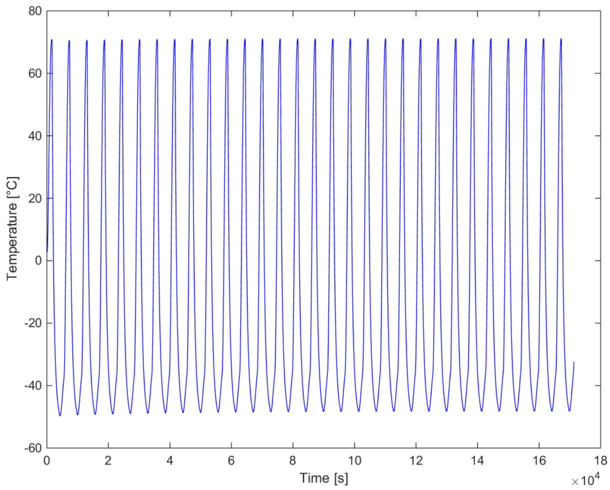

Figure 72: Temperature of Lateral panel (-X)

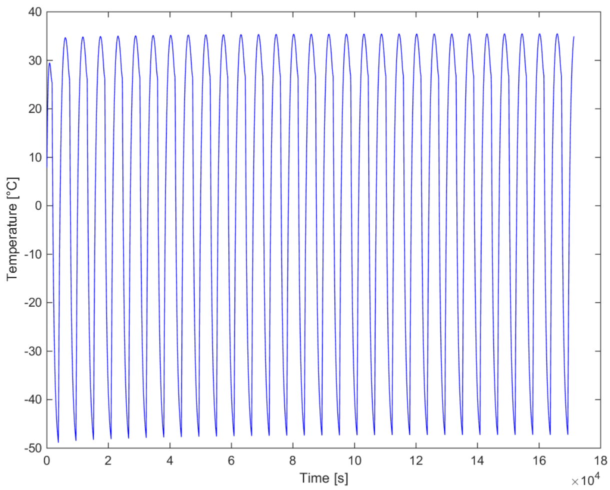

Figure 73: Temperature of Lateral panel (-Y)

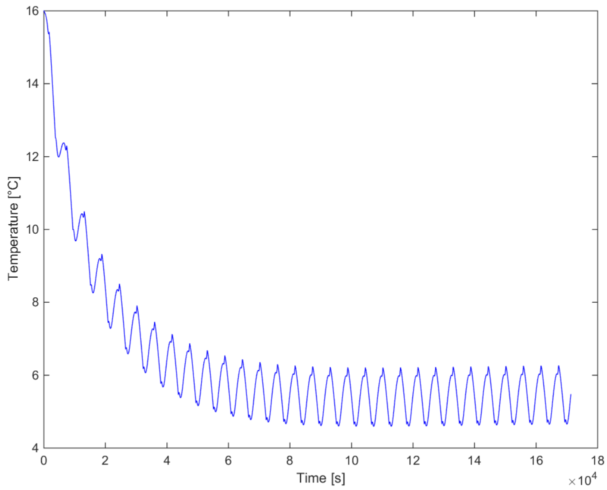

Figure 74: Temperature of Bottom panel

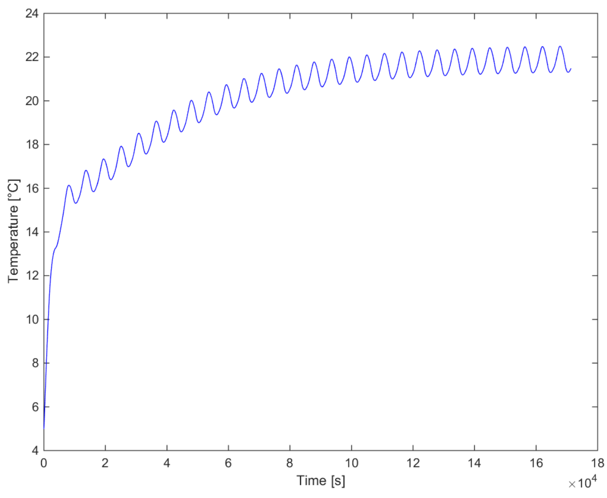

Figure 75: Temperature of Tray 6_2 bottom

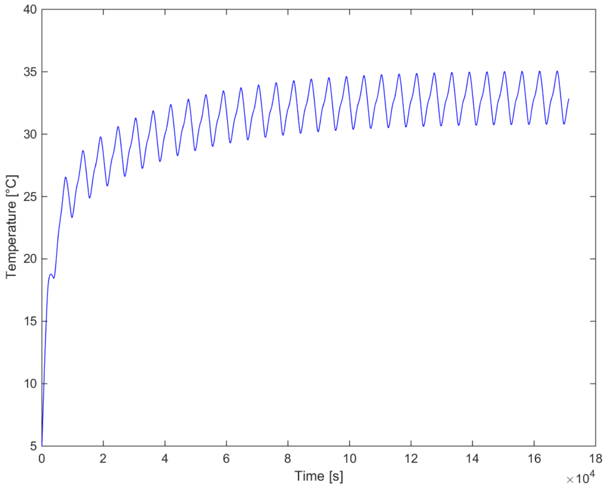

Figure 76: Temperature of Tray 6_1 bottom

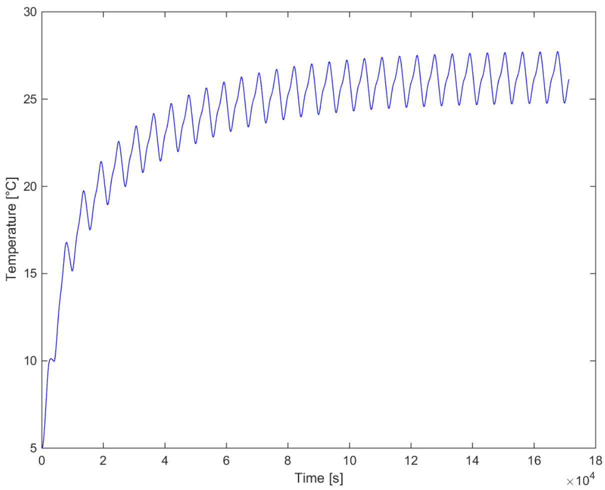

Figure 77: Temperature of Tray 5 bottom

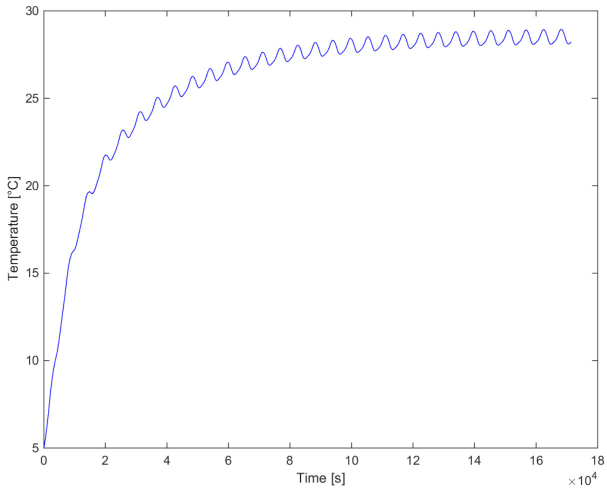

Figure 78: Temperature of Tray 4 bottom

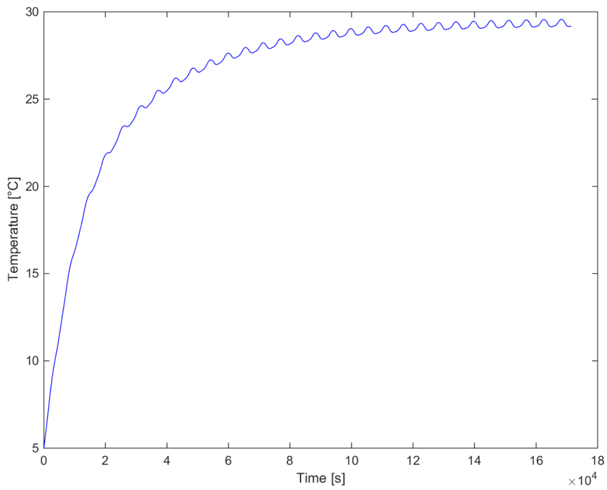

Figure 79: Temperature of Tray 3_3 bottom

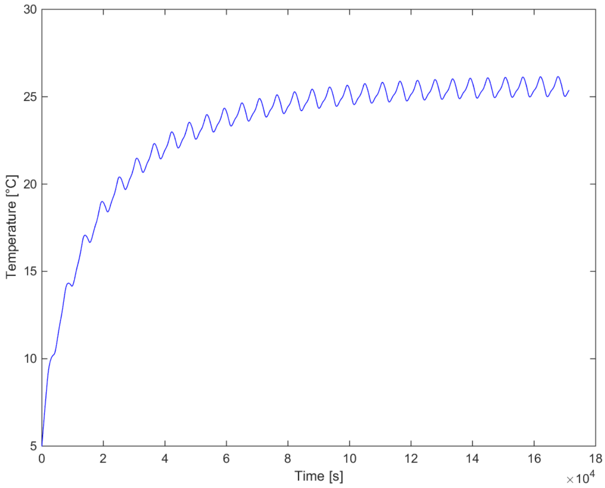

Figure 80: Temperature of Tray 3_2 bottom

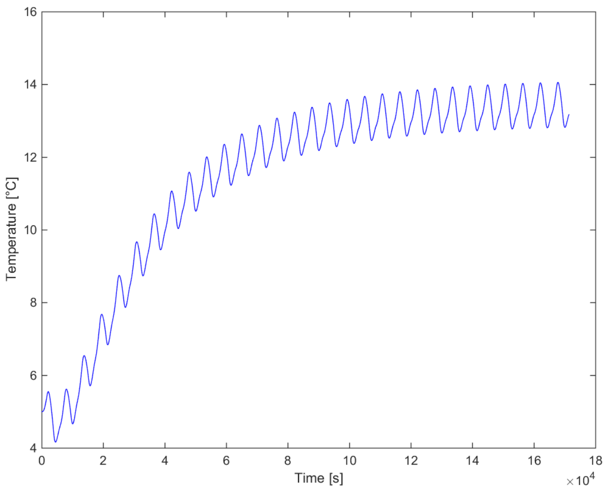

Figure 81: Temperature of Tray 3_1 bottom

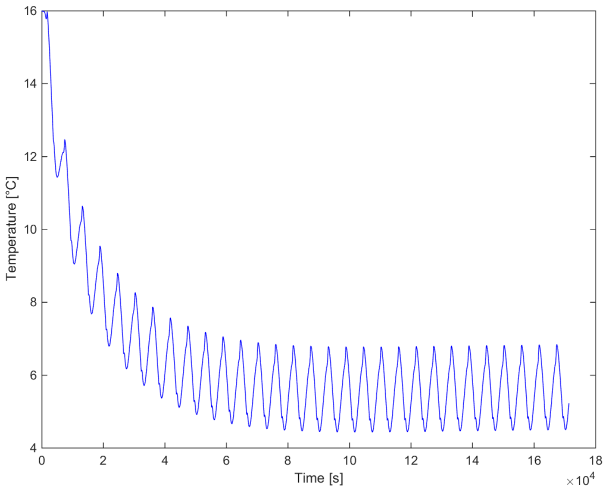

Figure 82: Temperature of Sector 3 bottom

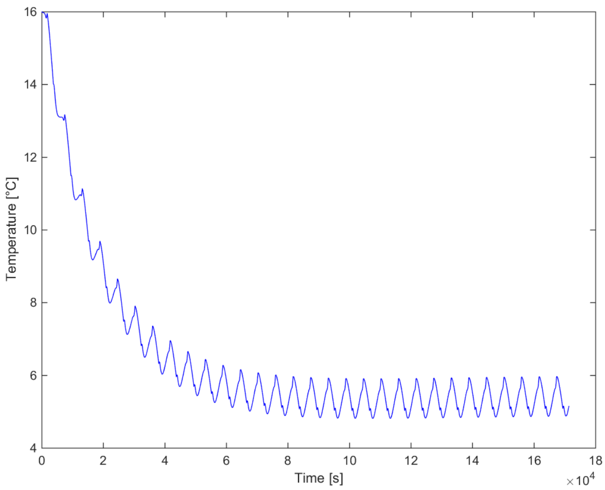

Figure 83: Temperature of Sector 2 bottom

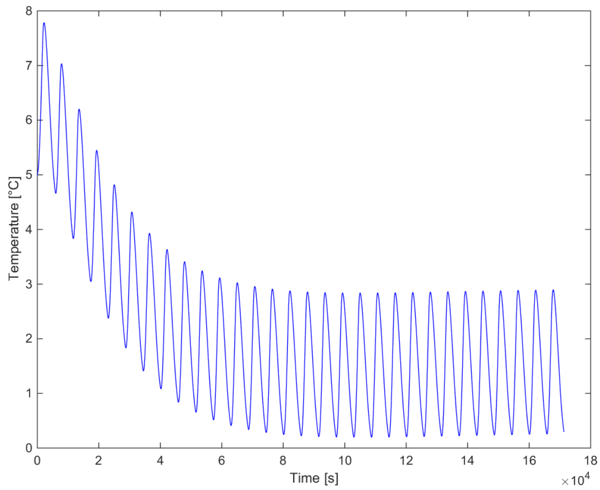

Figure 84: Temperature of HSTX

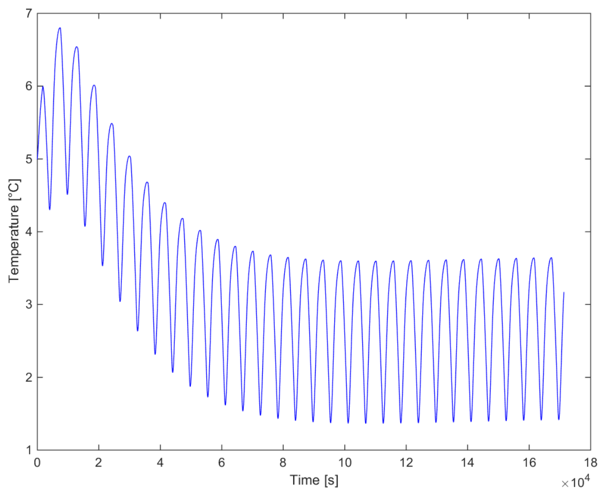

Figure 85: Temperature of AMSAT

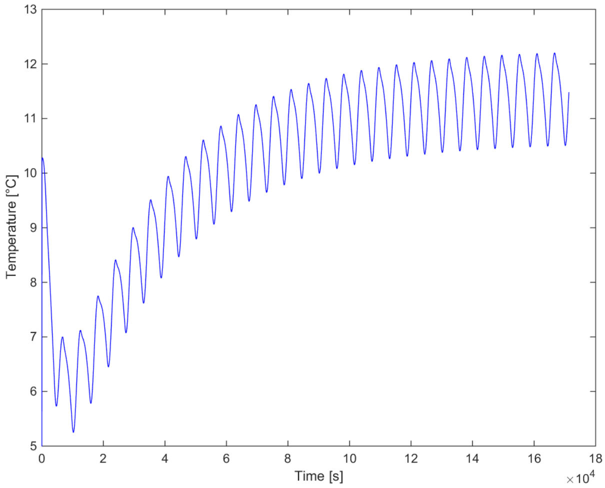

Figure 86: Temperature of DOM

ESEO Power Simulator

Just like many other systems, a satellite needs electrical power to operate. In the Earth there are many ways to produce electrical power but when one is out in space the problem is where to get that power from.
The Sun is a very powerful, clean and convenient source of power, particularly for satellites and an efficient way to convert the energy contained in the Sun's radiation into electrical power is by using panels composed of semiconductor *Photovoltaic Cells* (PV). During the eclipse, the solar panels cannot produce electrical energy and the satellite would not be able to operate if a backup power source were not available. Electrical energy therefore has to be stored on-board the spacecraft when in sunlight for consumption during these eclipses. The most widely used energy storage technology is the battery, based on reversible chemical reactions.
The scope of the simulator is to verify that the satellite power consumption, in all operational modes, with the orbit chosen and the solar panels temperatures, is compatible with the power budget.
The block diagram in Figure 87 represent a simple scheme of a power system simulator; left to right it shows the solar panels, the regulator and the battery packs. According to the battery voltage the regulator fixes the correct current generated by the solar panels and necessary to power satellite components and to recharge the battery packs. The load block models the power drawn by subsystems and payloads.

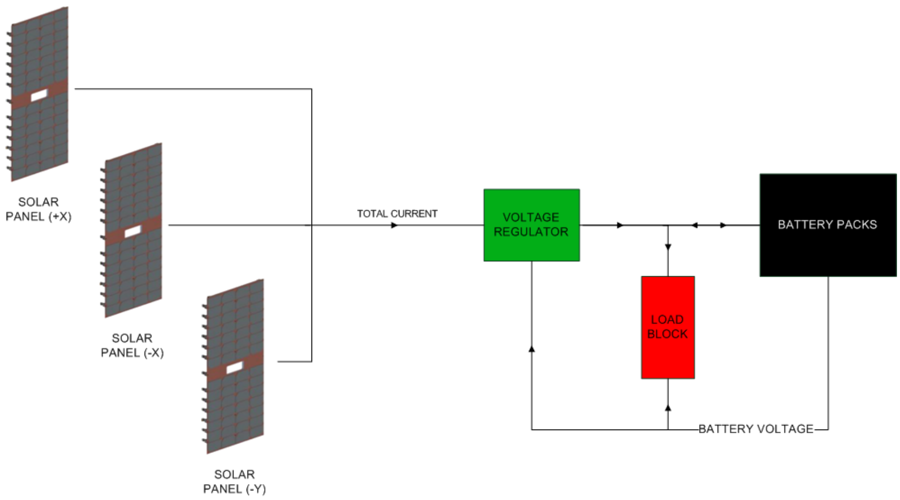

Figure 87: The power system simulator block diagram

The overall architecture of the model, which is based on a pre-existing power simulator implemented in Simulink, is reported in Figure 88. The arrangement and the colour of each subsystems is the result of the choice of remaining consistent with the block diagram previously reported.
In the next sections we will analyse these blocks in more detail.

7.1 Solar Panel

The solar array is made of numerous PVs combined to produce the amount of electric power needed for a satellite to function and to meet the power demands of its on-board instruments. A photovoltaic cell in practical use consists of a semiconductor, mostly silicon, doped in two different ways in order to create the so called *P-N junction*. In the P-region, the initially pure and electrically neutral silicon is doped with atoms and gets free holes. On the contrary the N-region silicon gets electrons in excess. First, a large

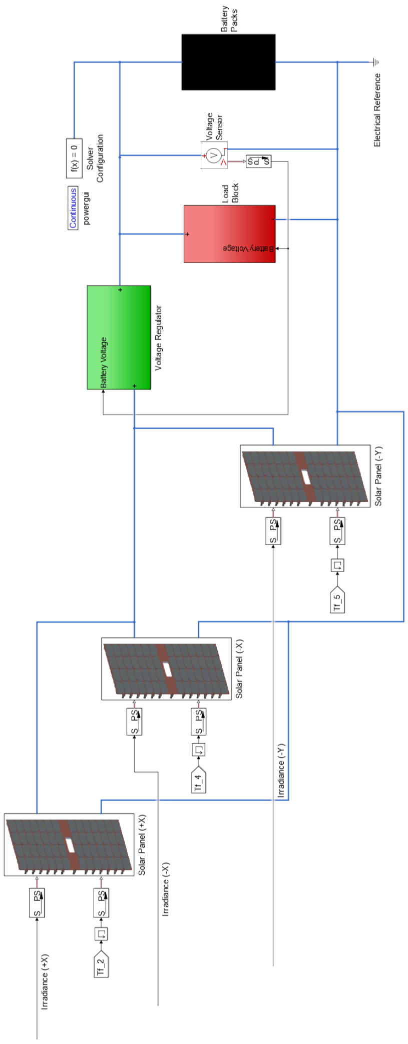

Figure 88: The power system simulator in Simulink

gradient exists between both sides and some free electrons from the N-region move toward the P-region and go across the junction while some free holes go from the P-side to the N-side (Figure 89). This process progressively build-up a positive charge in the N-region as well as a negative charge in the P-region and continues until an equilibrium state is reached. Then a potential barrier exists between both sides and the charges can no longer go through the junction without some extra energy. In our case, this energy is brought by the sunlight.

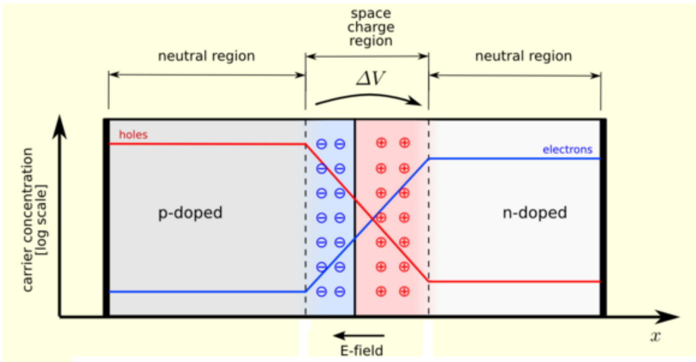

Figure 89: P-N junction

In ESEO a solar panel consists of 56 *AZUR SPACE Triple Junction GaAs* solar cells (Figure 90) arranged in 4 parallel strings, each one formed by 14 PVs in series. This cell type is an *InGaP/GaAs/Ge* on *Ge* substrate triple junction solar cell assembly (efficiency class 28%). All the design, mechanical and electrical data are reported in a proper data sheet [18]. They are referred to an incident irradiance equal to $1367\frac{W}{m^2}$ and a measurement temperature equal to $28\ ^{\circ}C$.

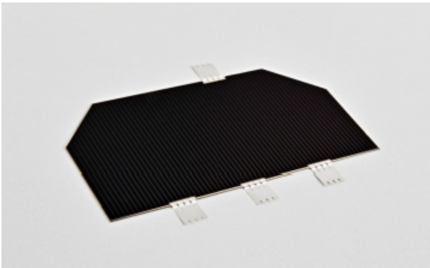

Figure 90: AZUR SPACE 3G28A [18]

How to model it?

The steady state equivalent circuit in Figure 91, represents the complex physics of a PV cell.

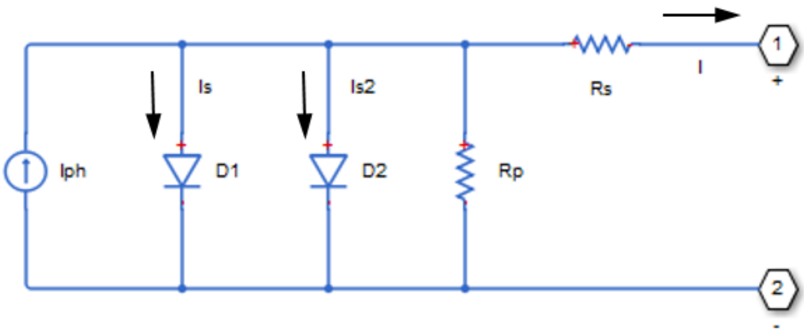

Figure 91: Cell equivalent circuit [10]

An ideal cell is modelled as a current source (I_{ph}: solar induced current) in parallel with a perfect diode ($D1$). In practice no solar cell is ideal and for taking into account different properties, it is necessary to consider additional elements:

- A second diode ($D2$) in parallel that models the *recombination effect* in the junction;

- A series resistance (R_s), introduced to consider internal losses in due to flow of current;
- A parallel resistance (R_p) that models the *leakage current* to the ground when diode is in reverse biased.

Te output current I is:

$$I = I_{ph} - I_s(e^{\frac{V+IR_s}{NV_t}} - 1) - I_{s2}(e^{\frac{V+IR_s}{N_2 V_t}} - 1) - \frac{V + IR_s}{R_p} \tag{7.1}$$

where:

- I_s is the saturation current of the first diode;
- I_{s2} is the saturation current of the second diode;
- V_t is the thermal voltage;
- N is the quality factor of the first diode;
- N_2 is the quality factor of the second diode;
- V is the voltage across the solar cell electrical ports.

This model is fully implemented in Simulink with a block called *Solar Cell* and, by default, it has the following ports:

- I_r: incident irradiance;
- $+$: positive electrical voltage;
- $-$: negative electrical voltage.

An additional port (*Thermal port*) can be exposed. It represent just the thermal mass of the device and it is used in order to fix the temperature of the cell with an external physical signal.
Moreover, it is possible to configure this Simulink block in three different ways [10]:

- **By s/c current and o/c voltage, 5 parameter**: It provides short-circuit current and open-circuit voltage that the block converts to an equivalent circuit model of the solar cell;
- **By equivalent circuit parameters, 5 parameter**: It provide electrical parameters for an equivalent circuit model of the solar cell with the following assumptions:
  - The saturation current of the second diode is zero;
  - The parallel resistor has infinite impedance.
- **By equivalent circuit parameters, 8 parameter**: It provides electrical parameters for an equivalent circuit model of the solar cell using the 8-parameter solar cell model.

Considering the available parameters in the data sheet we have been chosen the first type of configuration (Figure 92).
However, as we reported before, a solar panel is a proper combination of solar cells and in particular we have 4 strings each of these with 14 cells. The implementation of this arrangement in Simulink is reported in Figure 93. In this last figure, only one solar cell block for each string is present, since it is possible to model any number of PVs connected in series using a single block. It is sufficient to set the parameter *Number of series cells* to a value larger than 1 (in our case it is equal to 14). *Internally the block still simulates only the equations for a single solar cell, but scales up the output voltage according to the number of cells. This results in a more efficient simulation than if equations for each cell were simulated individually* [10].
In the end, the contribution of each solar panel in the power simulator must be taken into account, as depicted in Figure 94.

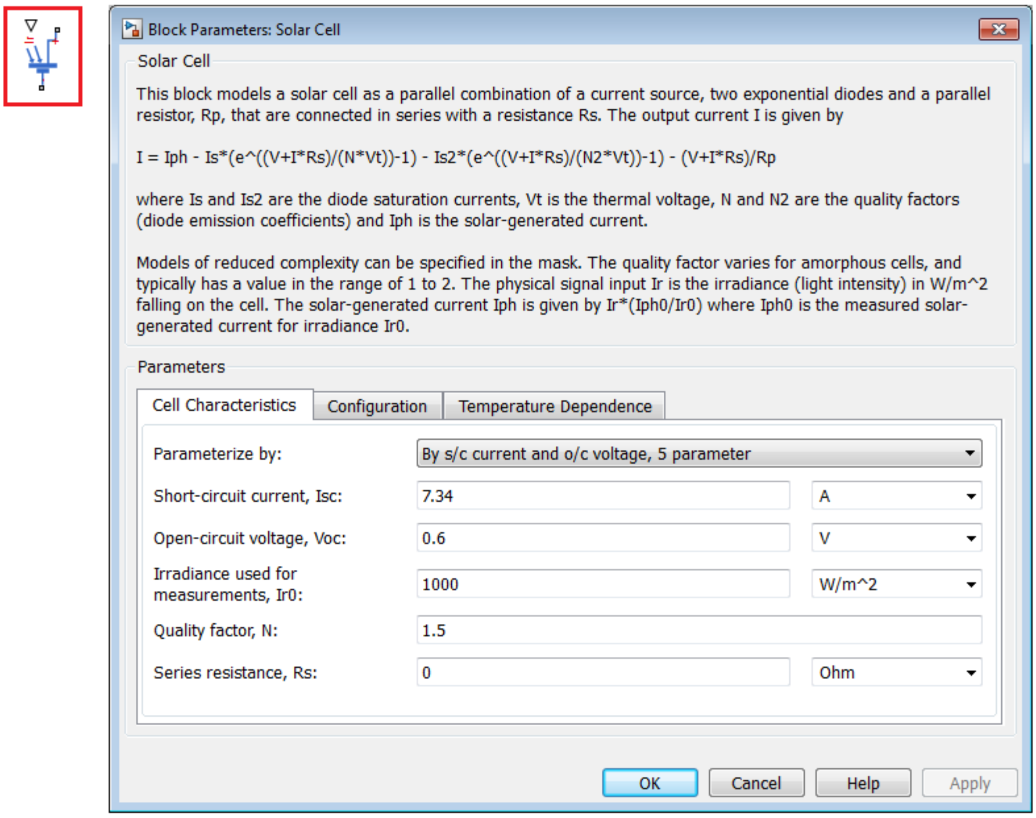

Figure 92: Solar Cell Block [10]

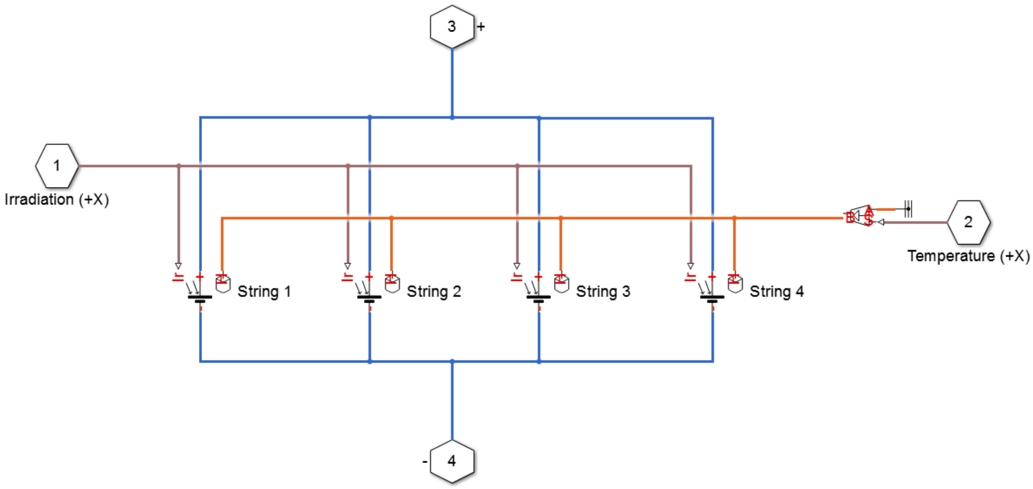

Figure 93: Solar Panel (+X)

7.2 Voltage Regulator

The purpose of this block is to insert the correct value of current inside the electrical circuit according to the battery voltage. In particular once this value exceed a proper upper threshold, the current is equal to that generated by the solar panels. This remains valid until the battery voltage is not lower than a specific limit and the current assumes a minimum value, according to the battery type.

How to model it?

There are two fundamental steps in order to implement the behaviour of the voltage regulator (Figure 95):

- **Step 1**:
  Create a combination of Simulink blocks that are able to

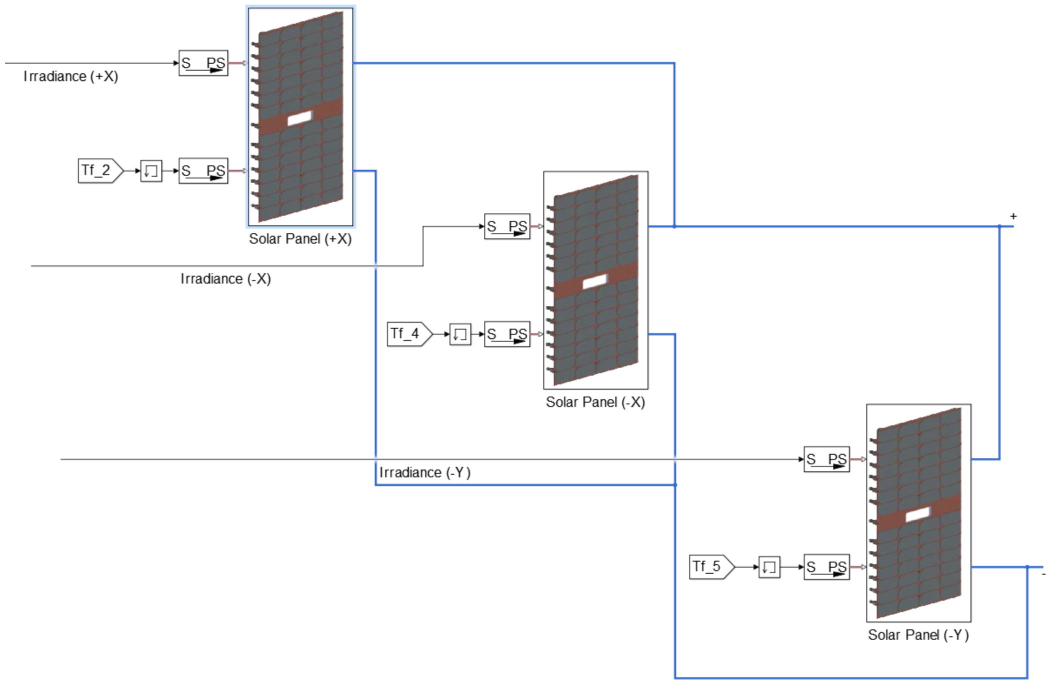

Figure 94: Solar panels combination

insert in the electrical circuit the correct current value. This is possible by means of a *Single-Phase Switch* block and a *Controlled Current Source* block in parallel with the solar panels. In this last block the value of the current to generate is provided by a switch;

- **Step 2**:
  Create the correct signal that drives the Single-Phase Switch and the Switch block. This is possible by the use of the *Relay* block that *remains on until the input drops below the value of the Switch off point parameter. When the relay is off, it remains off until the input exceeds the value of the Switch on point parameter* [10].
  Moreover when the Single-Phase Switch is close (so in the circuit flows the output of the solar panels) the current generator has a zero value in input, otherwise a value of $0.01A$ is generated once the contribution of the solar panels is left out the circuit.

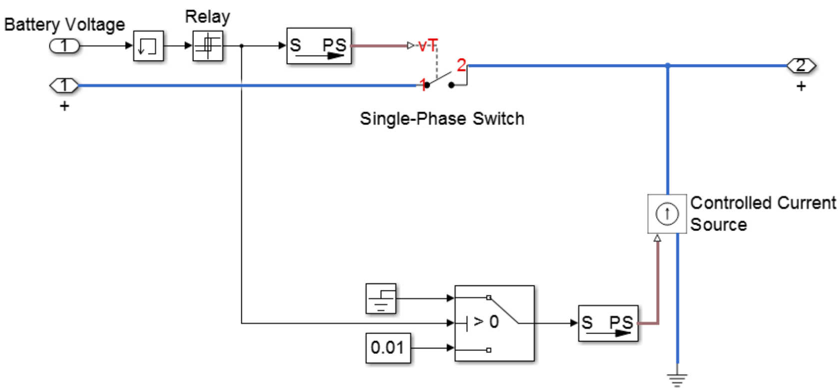

Figure 95: Inside Voltage Regulator subsystem

7.3 Load Block

The load block is used to simulate the energy consumption of subsystems and payloads during all the operative modes of the satellite.

7.3.1 How to model it?

A generic load can be modelled as an electrical resistance with a proper value. Running current through it, creates heat in a phenomenon called *Joule heating*:

$$P = VI$$

where P is the power in W converted from electrical energy to thermal energy, R is the resistance in Ω and I is the current in A that flows through the resistance.
According to these, it is possible to implement a variable resistance ,in parallel with the battery, with a value that changes in order to dissipate a power equal to that requested from the satellite (Figure 96).
Knowing the battery voltage ($V_{battery}$) and the value of the power ($P_{satellite}$), it is possible to find the value of the current (I_{load}) that flows through the resistance (R_{load}):

$$I_{load} = \frac{P_{satellite}}{V_{battery}} \Rightarrow R_{load} = \frac{V_{battery}}{I_{load}}$$

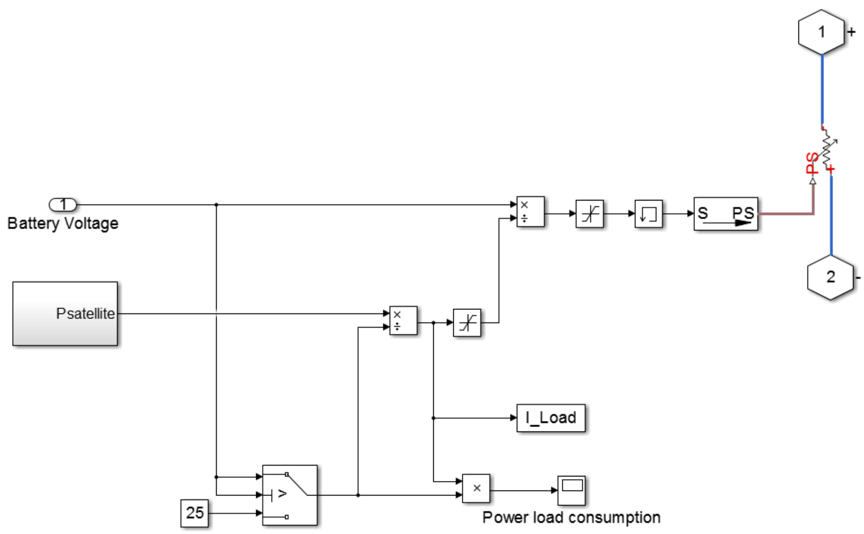

Figure 96: Inside Load Block subsystem

7.4 Battery Block

Electrical energy has to be stored on-board the spacecraft when in sunlight for consumption during the eclipses and the most widely used energy storage technology is the rechargeable battery. Composed of two or more electrochemical cells, it can be charged, discharged into a load, and recharged many times. Several different combinations of electrode materials and electrolytes are used but in our case we consider six *Lithium-Ion* batteries.

7.4.1 How to model it?

Simulink already implements a block that model the behaviour of several battery types. However an important thing to do is to modify the default Simulink block in order to closely match the battery model as found inside the starting version of the power simulator. Hence, the inputs (positive and negative terminal) must be transformed in physical signals with proper Simscape blocks (Figure 97).
The outputs m is a vector containing three signals: the battery voltage (*V_batt*), the battery current (*I_batt*) and the *State Of Charge* (SOC). This last signal is simply replaced by an alternative parameter: *Depth Of Discharge* (DOD). It is the complement of SOC and it is 0% when the battery is fully charged, 100% when it is fully discharged (Figure 98).

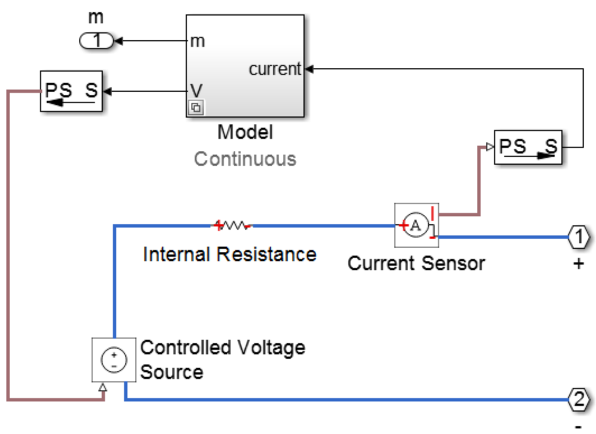

Figure 97: Battery model [10]

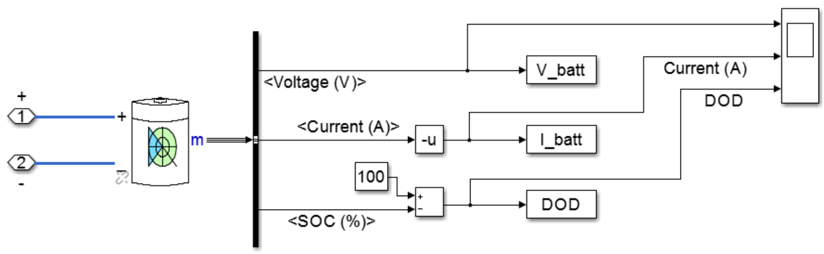

Figure 98: Inside Battery Packs

7.5 Validation Phase

For the validation of the simulator we have to compare the results of our model with those produced by the Power Simulator developed in SITAEL. The most important difference between these two simulators is related to how solar panels are modelled. Initially the solar panel was modelled through an ad-hoc developed internal Matlab function having as input the characteristics of the solar cells and their arrangement. As we already reported, in order to remain coherent with the method used for the thermal model, in our simulator a PV is implement with the Solar Cell Simscape block. However this has also the following advantages:

- Reduce of the 35% of the simulation time;
- More intuitive comprehension of how a solar panel is modelled.

For a correct validation matching of the same boundary conditions is fundamental and, in this case, we consider [16]:

- The orbital parameters of the ESEO orbit (Table 1);

Detumbling mode	19.05 W
Nominal sunlight mode	27.34 W
Nominal eclipse mode	24.75 W

Table 6: Platform total consumption

- A simulation time of 14 orbits;
- A detumbling phase of 3 orbits with no battery recharge;
- A constant solar flux of $1367\frac{W}{m^2}$;

- Platform total consumption with system margin reported in Table.
- Temperature of the cells computed through the simplified thermal model without interaction between external panels and spacecraft platform, as found in the original ESEO Power Simulator. Moreover we consider solar cells also for the side +Y.

Finally the comparison of output of the models, reported from Figure 99 to 101; they underline a good agreement of the outputs of the battery block.

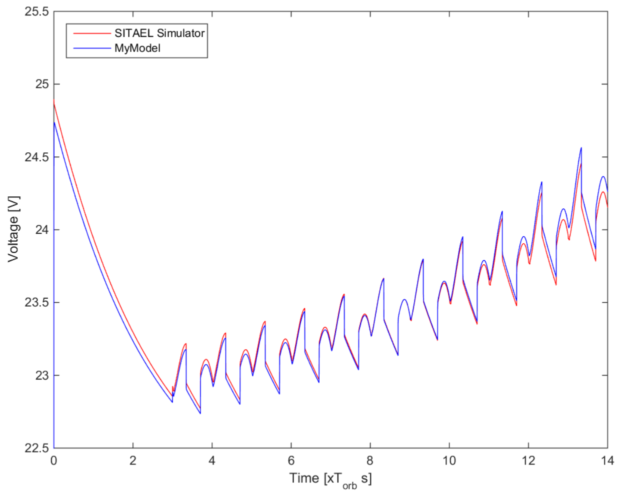

Figure 99: Comparison of Battery voltage

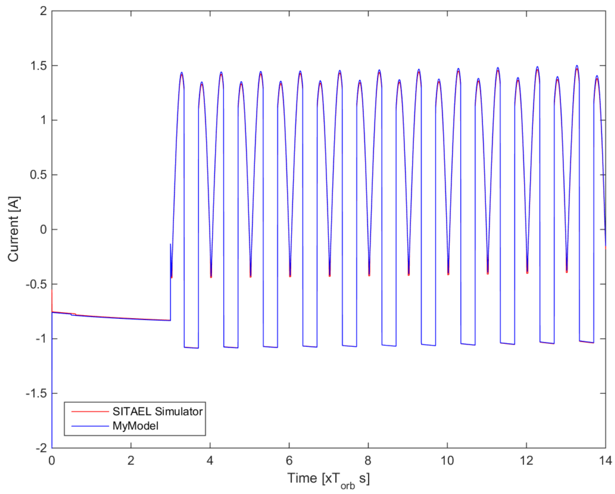

Figure 100: Comparison of Battery current

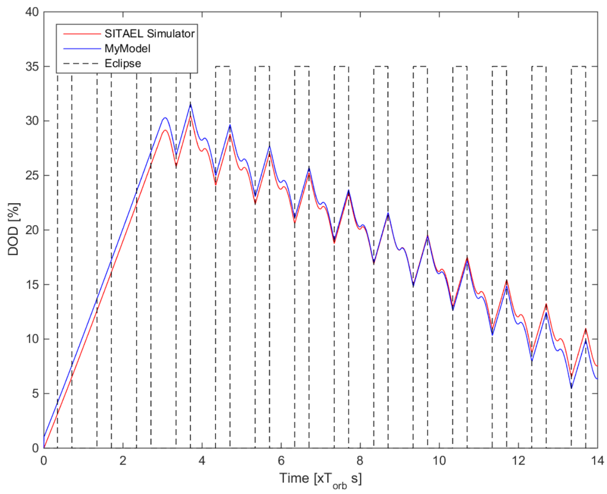

Figure 101: Comparison of Battery DOD

Interface Block

ESEO satellite is able to communicate with the ground station (GS) through radio signals. This is important not only for obtaining science data, for which the mission was designed, but also useful information, from an engineering point of view, about the health of the spacecraft and its subsystems.
The work, done during the thesis preparation [19] and briefly summarized in this chapter, derives from the necessity to design a system capable of receiving a message from the GS, converting it in a specific request and sending the correct response, interacting with the spacecraft simulator. In Figure 102, a schematic representation of the functional blocks for the interface between the ground segment and the satellite simulator is depicted (the red box being the subject of the present work).
On the left there is the Ground Segment PC characterized by these elements:

- **Mission Control System:** it represents the handling system of the commands (TC)/telemetry data (TM);

- **SDR Software:** it elaborates a *baseband signal* (BB) which has to be transmitted or received through URSP N210. Regarding this device, the uplink frequency (UP) is 435.2 MHz while the downlink one (DWN) is 437 MHz.

On the right, the block called Satellite/Simulator PC, simulates the behaviour of the satellite when it receives a radio signal from the GS. In particular it consists of:

- **Satellite TMTC and OBDH Simulator:** the former simulates the processing of the received/sent signals through the USRP N210 device (inverted frequency). The latter simulates the behaviour of the satellite when it receives a command ans sends TM data, in particular, the check system of the input message. If all is ok the command is elaborated otherwise, the OBDH (On-Board Data Handling) sends a reject message to the GS;

- **Interface Block and Spacecraft Simulator:** it represents, in particular the former, the work done and it will be widely analysed in the following sections.

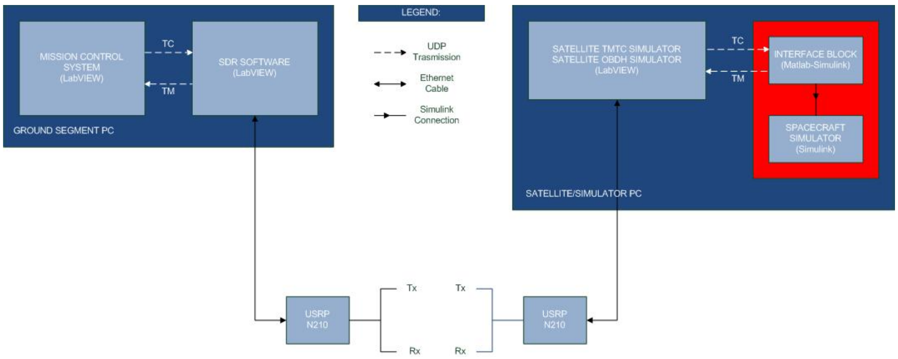

Figure 102: Telecommunication System [19]

Moreover, for TC and TM we used an *User Datagram Protocol* (UDP), a simple connectionless transmission model that has no handshaking dialogues. Thus, there is no guarantee of delivery, ordering or duplicate protection. Beyond this drawback, overcome by the fact that we work in localhost, UDP is a very fast and easy transmission protocol.

8.1 Types of message for the satellite

The types of message that a satellite can receive (send) from (to) the GS are reported in the next two sections.

8.1.1 Received command

It is a string of seven bytes, in hexadecimal notation, subdivided as follows:

Address	**Type**	**Register**
2 bytes	1 byte	4 bytes

Table 7: Received Message Structure

- **Type:** it can be only *0x01* or *0x10*. The former identifies a SET command that, in general, assigns a specific variable, defined by the Address field. The latter characterizes a GET command used for evaluating a variable;
- **Address:** the first byte uniquely identifies the equipment (ACS, PMM, OBD, ...) while the second byte identifies the specific parameter within ACS, PMM, ...
- **Register:** it has no meaning in case of a GET command, instead for a SET one, it contains the value we want to assign. In general it can be represented with a certain number of bytes according to its class:
  - **uint8/int8:** 1 byte;
  - **uint16/int16:** 2 bytes;
  - **uint32/int32:** 4 bytes;

- **SGL:** 4 bytes;
- **DBL:** 8 bytes.

Since the Register can not represent a value of a variable in double precision, it has to be assigned with two commands (see Section 4.3.2).

When the action of assignment of a variable is done immediately after the received message we call it *Immediate* o *Standard*; for a SET command, it can also be *Time Tagged*. In this case, the OBDH simulator stores it in a on-board schedule and processes it only after that a specific amount of time, contained in the received message, is elapsed. Thanks to this fact, from the Interface Block point of view, a command of this kind is considered like Standard because it is received exactly when it has to be performed.
A realistic example of the use of a Time Tagged command is when a LEO satellite can not establish a connection with the GS while it is orbiting over a point of interest for the mission. It is therefore necessary, also for energy saving reasons, to enable the camera only for a certain time.
Lastly we have to underline that a SET command, associated with Address *0x000F* (*HK and TC Management*), can activate two important requests for satellite health monitoring:

- **HK Data Page:** we can obtain simultaneously a group of data of the same *Equipment* collected in a specific page;
- **HK History Page:** represents an extension of the HK Data Page because, in this case, we download all the pages from the oldest (Tnow-660 minutes) to the latest (Tnow) in this order:
  - Tnow-660min: From pag.1 to...
  - Tnow-650min: From pag.1 to...

- ...
- Tnow: From pag.1 to...

8.1.2 Sent message

For every kind of received message, we always have, as response, an *Acknowledge* (ACK) or a *Reject* (REJ) followed by a specific stream of data in case of HK Data Page or HK History Page.
A message sent from the Interface Block to the OBDH simulator has a fixed dimension of 128 bytes and can be of these types:

- **ACK**

		Data Field			
Class 1 byte	**Length** 1 byte	**Type** 1 byte	**Address** 2 bytes	**Register** 4 bytes	Filled until 128 bytes

Table 8: ACK Structure

- **Class:** it distinguishes an ACK (or REJ) from an HK Data Page (or HK History Page) and, in the former case, is fixed to *0x02*;
- **Length:** it identifies the length of the *Data Field*;
- **Type:** fixed to *0x01* in case of ACK;
- **Address:** already explained in Section 2.2;
- **Register:** formed by 4 bytes, in case of a GET command it represents the value of the variable, identified by the Address, while, in case of a SET command, it represents a copy of the Register of the received message.

		Data Field		
Class 1 byte	**Length** 1 byte	**Type** 1 byte	**Error** 2 bytes	Filled until 128 bytes

Table 9: REJ Structure

- **REJ**
  - **Class:** as we have seen previously, it is fixed to *0x02*;
  - **Length:** like in ACK;
  - **Type:** in this case it is a byte fixed to *0x10*;
  - **Error:** in hexadecimal notation, it identifies the reason of the rejection.
- **HK Data Page**

		Data Field		
Class 1 byte	**Length** 1 byte	**Page number** 1 byte	**Page content** n bytes	Filled until 128 bytes

Table 10: HK Data Page Structure

  - **Class:** it is a byte fixed to *0x09*;
  - **Length:** it represents always the number of bytes of the Data Field;
  - **Page number:** it is a byte that identifies, in hexadecimal notation, the number of the requested page;
  - **Page content:** it is the content of the page defined in the earlier field.

		Data Field				
Class	**Length**	**HK set time**	**HK set number**	**Page number**	**Page content**	
1 byte	1 byte	6 bytes	1 byte	1 byte	n bytes	Filled until 128 bytes

Table 11: HK History Page Structure

- **HK History Page**
  - **Class:** in this case, this byte is fixed to *0x0A*;
  - **Length:** like in the past categories of message;
  - **HK set time:** represents the information about the time when the values, included in the pages, are assessed. This field, formed by six bytes in hexadecimal notation, is so defined:

Byte 5	**Byte 4**	**Byte 3**	**Byte 2**	**Byte 1**	**Byte 0**
Days after J2000			Seconds of the day starting from noon		

Table 12: HK set time Structure

  - **HK set number:** is the content of the page defined in the earlier field and identifies the stream of messages from a chronological point of view. It varies from *0x01* (the older) to *0x42* (the latest);
  - **Page number:** like in HK Data Page;
  - **Page content:** like in HK Data Page.

8.2 Inside the Interface Block

This is a fundamental block and it models a system capable of receiving a message from the GS, converting it in a specific request and sending the correct response, interacting with the spacecraft. It consists of five important groups (Figure 103):

- **Group A:** formed by a subsystem, called *Receive Message*, it receives the command from the Satellite TMTC and OBDH Simulator;
- **Group B:** formed by the *Send Message* subsystem and a set of SIMULINK blocks, it sends the correct message at the command;
- **Group C:** it determines the acknowledge of the command, in fact, it is formed by a subsystem, called *ACK*;
- **Group D:** it represents the connection point from Interface Block and Spacecraft Simulator, needed for the assignment of a variable;
- **Group E:** it implements the request of HK Data Page or HK History Page.

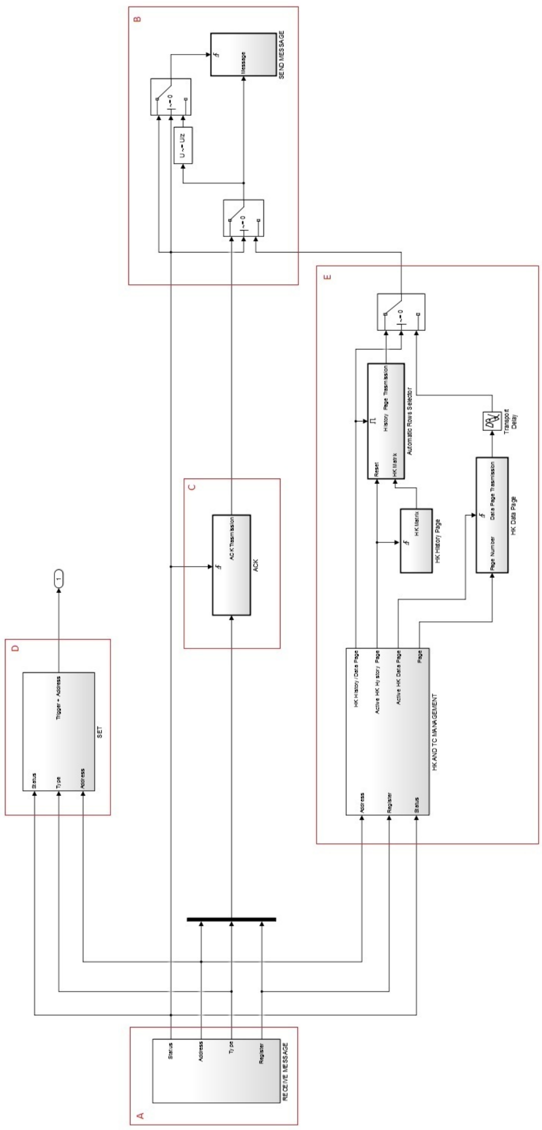

Figure 103: Inside Interface [19]

8.3 Some possible applications

The implementation of this block in our simulator is very important because it makes possible to obtain data not only related to the attitude of the satellite but also to the Thermal and Power subsystem.
Moreover with a standard SET command it is possible to switch on or off a particular payload or unit and to analyse how it affects from the thermal or power point of view.

Conclusion

In this thesis we tried to develop a simulator that models in a proper way aspects related to the Thermal and Power Subsystem. Moreover, a communication link between the simulator and the ground segment has been implemented and verified through the development of an Interface Block.
Successive work could involve the extension of the simulator in order to model other spacecraft subsystems and to obtain, at the end, a complete interactive ESEO satellite simulator.

Acknowledgments

The pictures of ESEO, some software and reference documents employed during this thesis are proprietary material of SITAEL, whose support is acknowledged.

Bibliography

[1] Space in images, *ESEO Model*, European Space Agency, 2015, http://www.esa.int/spaceinimages/Images/2015/04/ESEO_model

[2] Davide Bruzzi, Nicola Melega, Paolo Tortora, Fabrizio Giulietti, Piero Galeone, Antonio De Luca, *The ESEO mission: current status and achievements*, 10th Symposium on Small Satellites for Earth Observation (Berlin), 2015

[3] Frank P. Incropera, *Fundamentals of heat and mass transfer*, John Wiley & Sons, 2011

[4] John H. Lienhard, *A heat transfer textbook*, Phlogiston press, 2015

[5] MSFC Engineering Directorate, *Guidelines for the selection of near-Earth thermal environmental parameters for spacecraft design*, NASA, 2001

[6] Antonio De Luca, *Architectural Design Criteria for Spacecraft Solar Arrays*, InTechOpen, 2011

[7] Davide Bruzzi, Paolo Tortora, Piero Galeone, *European Student Earth Orbiter: ESA's educational Microsatellite Program*, 27th Annual AIAA\USU. Conference on Small Satellites, 2013

[8] AS\12_0005\SYS\AR-01, *System Design Report*, SITAEL SpA, 2013

[9] Miguel Á. C. Perpiñán, *The modelling of the thermal subsystem in spacecraft real-time simulators*, ESA-ESOC, 1994

[10] *Simscape User's Guide*, MathWorks, 2015

[11] Developers of Thermal Analysis Kit (TAK), *Thermal Network Modeling Handbook*, K&K Associates, 2000

[12] B. Gebhart *Surface temperature calculations in radiant surroundings of arbitrary complexity for gray, diffuse radiation*, International Journal of Heat and Mass Transfer, 1961

[13] John R. Howell*A catalog of radiation heat transfer configuration factors*, University of Texas, www.thermalradiation.net/tablecon.html

[14] AS\12_0005\SYS\PLA\STR-AR-01, *STR Subsystem Design Definition File*, SITAEL SpA, 2014

[15] AS\12_0005\SYS\AR-05, *Thermal Design Report*, SITAEL SpA, 2014

[16] AS\12_0005\PS\DDF-01, *Power System Simulator*, SITAEL SpA, 2014

[17] Gregory Nellis and Sanford Klein, *Heat Transfer\Example 10.5-2*, Cambridge University Press, 2008

[18] AZUR SPACE *28% Triple Junction GaAs Solar Cell Assembly*, Data Sheet

[19] Alberto Lucci, *Thesis Preparation*, 2015